Crystal structure and activity profiling of deubiquitinating inhibitors-bound to SARS-CoV-2 papain like protease revealed new allosteric sites for antiviral therapies

Shweta Choudhary[1], Sanketkumar Nehul[1], K Amith Kumar[1], Swati Sharma[1,2], Ruchi Rani[1], Ankita Saha[1], Gaurav Kumar Sharma[3], Shailly Tomar[1*], Pravindra Kumar[1*]

[1]Department of Biosciences and Bioengineering, Indian Institute of Technology Roorkee, Uttarakhand (247667), India.
[2]Shiv Nadar University, Uttar Pradesh, (201314), India
[3]Indian Veterinary Research Institute, Izatnagar, Bareilly, Uttar Pradesh (243122), India

***Corresponding author details**

Shailly Tomar*
Professor,
Department of Biosciences and Bioengineering,
Indian Institute of Technology Roorkee,
Uttarakhand, India 247667
Tel: +91-1332-285849
Fax: 91-1332-273560
Email: shailly.tomar@bt.iitr.ac.in
ORCID ID: 0000-0002-1730-003X

Pravindra Kumar*
Professor and Head of the Department,
Department of Biosciences and Bioengineering,
Indian Institute of Technology Roorkee,
Uttarakhand, India 247667
E-mail: pravindra.kumar@bt.iitr.ac.in
Telephone: +91-1332-286286
ORCID ID: 0000-0003-2128-7736

Gaurav Kumar Sharma
Senior scientist,
Centre for Animal Disease Research and Diagnosis (CADRAD),
Indian veterinary Research Institute, Bareilly (IVRI, Bareilly)
Uttar Pradesh, India
Telephone: 0581-2302188
Email: gaurvet@gmail.com
ORCID ID: 0000-0002-9996-9422

Abstract

Emerging variants of SARS-CoV-2 still threaten the effectiveness of currently deployed vaccines, and antivirals can prove to be an effective therapeutic option for attenuating it. The papain-like protease (PLpro) is an attractive target due to its sequence conservation and critical role in the replication and pathogenesis of SARS-CoV-2. PLpro also plays very important role in modulation of host immune responses by deubiquitinating (DUBs) or deISGylating host proteins. Thus, targeting PLpro serves as a two-pronged approach to abate SARS-CoV-2. Due to its structural and functional similarities with the host DUB enzymes, an *in-house* library of DUB inhibitors was constituted in this study. Five promising compounds exhibiting high binding affinities with the substrate binding site of PLpro were identified from a library of 81 compounds with *in silico* screening, docking, and simulation studies. Interestingly, lithocholic acid, linagliptin, teneligliptin, and flupenthixol significantly inhibited the proteolytic activity of PLpro. Each of these compounds abrogated *in vitro* replication of SARS-CoV-2 with EC_{50} values in the range of 5-21 μM. In addition, crystal structure of SARS-CoV-2 PLpro and its complex with inhibitors have been determined that revealed their inhibitory mechanism. The findings of this study provide the proof-of-principle that the DUB inhibitors hold high potential as a new class of therapeutics against SARS-CoV-2. Additionally, this is the first study that has opened a new avenue towards not only targeting PLpro active site but also simultaneously directing towards restoration of antiviral immune response of the host for deterring SARS-CoV-2.

Graphical abstract

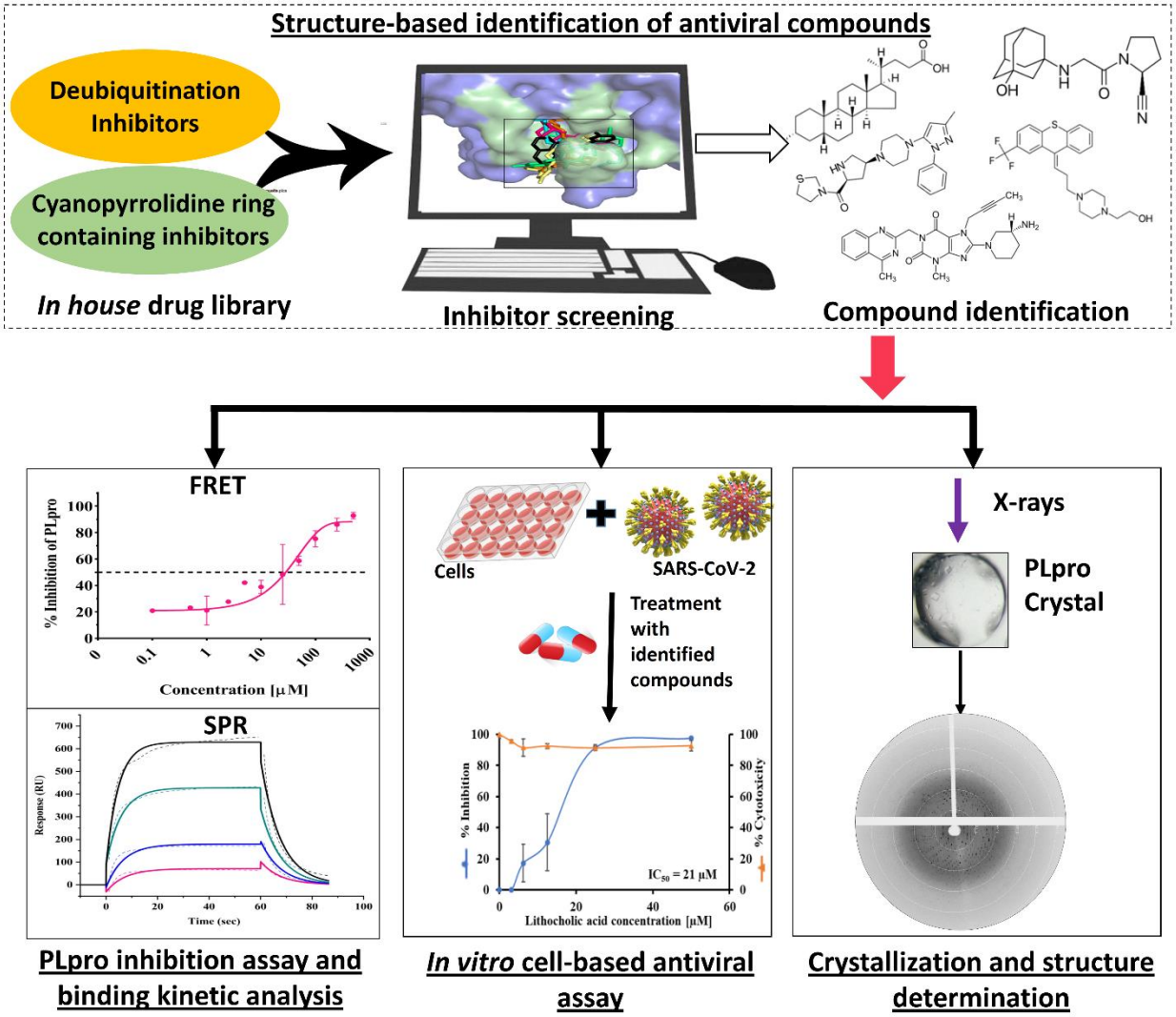

Introduction

The ongoing prevalence of COVID-19, caused by the novel SARS-CoV-2, has been ravaging for more than a year and has resulted in incalculable devastation of healthcare infrastructure. Despite the rapid rollout of effective vaccine-based prophylactic therapies against SARS-CoV-2, hopes for the imminent end of the pandemic are short-sighted, underscoring the immediate unmet need for safe and effective antivirals [1][2]. Crucially, the range, strength, and duration of vaccinal as well as natural immunity is still uncertain and is waning with time which could lead to breakthrough infections owing to highly transmissible variants [1][3][4][5]. The emergence of new variants of concern (VOCs) with a potential to escape therapeutic antibodies has also raised significant concerns about the geographical or temporal efficacy of these interventions [6][7][8].

The resurgence of new SARS-CoV-2 variants suggests a dearth need for the development of effective antivirals targeting highly conserved viral proteins to curtail the further spread of SARS-CoV-2 infections. Precedent studies on SARS-CoV-2 highlight that the catalytic site of certain non-structural proteins (nsP) of SARS-CoV-2, such as papain-like protease (PLpro), 3-chymotrypsin-like protease (3CL pro or Mpro), RNA-dependent RNA polymerase (RdRp), and helicase display high levels of sequence similarity with their corresponding SARS and MERS counterparts and represent attractive antiviral targets against SARS-CoV-2 [9][10][11][12]. Furthermore, due to the high degree of conservation of these nsPs among other coronaviruses, the probability of emergence of new mutations in these proteins is presumably low compared to the spike protein of SARS-CoV-2 [13]. Remdesivir, a RdRp inhibitor, has already been approved, while few Mpro inhibitors are currently in the phase of clinical trials (NCT04627532, NCT04535167) [9][14][15][16][17]. PLpro presents to be a more challenging and potentially promising druggable target of SARS-CoV-2, for which effective inhibitors are yet to be discovered [18].

The genome of SARS-COV-2 comprises a single-stranded positive-sense RNA of ~ 30kb, which is translated to produce structural, non-structural, and accessory viral proteins, essential for carrying out replication, maturation, and genome packaging of SARS-CoV-2 [19][20]. The genomic RNA gets translated to produce two overlapping polyproteins, pp1a and pp1ab (formed after -1 ribosomal frameshifting mechanism), that are proteolytically cleaved and processed into 16 nsPs by two virus-encoded cysteine proteases, the PLpro and the Mpro [21][22]. These nsPs form the replication and transcription complex (RTC) responsible for directing the process of transcription, replication, and maturation of the viral genome [19][20][23]. SARS-CoV-2 PLpro, a domain within nsP3 protein, is a cysteine protease that recognizes the P4-P1 consensus LXGG sequence and cleaves the peptide bond between nsP1/nsP2 (LNGG↓AYTR), nsP2/nsP3 (LKGG↓APTK), and nsP3/nsP4 (LKGG↓KIVN) [9][24]. It shares a sequence identity of 83% with PLpro of SARS-CoV and is relatively distant from MERS with a sequence identity of 32.9% [25][26]. As an evasion mechanism against the host innate immune response, PLpro possesses deubiquitination and deISG15ylation activities that cleave off ubiquitin and ISG15 (ubiquitin-like interferon-stimulated gene 15) post-translational modifications from host proteins by recognizing

the C-terminal RLRGG sequence [26][27][28]. SARS-COV-2 PLpro exhibits a different preference for host substrate, cleaving ISG15 more preferentially, whereas PLpro of SARS-CoV predominantly cleaves off ubiquitin chains [21][26]. Interestingly, the multifunctional PLpro inactivates TBK1, a kinase required to activate transcription factor interferon responsive factor 3 (IRF3), prevents dimerization and translocation of IRF3 to the nucleus, and blocks NF-κB signaling pathway, eventually attenuating the type I interferon response of the host cell [21][27][29]. Due to the role of PLpro in replication and pathogenesis of SARS-CoV-2, targeting PLpro may have an advantage in not only suppressing viral infection but also impeding the dysregulation of signaling cascades in infected cells that may lead to cell death in the surrounding, non-infected cells. GRL0617, a naphthalene-based molecule, is the only inhibitor reported to inhibit replication of both SARS-CoV and SARS-CoV-2 by targeting PLpro [30].

Of note, PLpro has a right-handed "thumb-palm-finger" architecture which is similar to that of host deubiquitinating enzymes (DUBs), the ubiquitin-specific protease (USP), despite very low sequence similarity between them (~10%) [21]. SARS-CoV-2 PLpro has two domains, the "thumb-palm-finger" catalytic domain at the C-terminus and a small N-terminal ubiquitin-like (UBL) domain [21][29][31]. The active site of PLpro is made up of a canonical cysteine protease triad of Cys111, His272, and Asp286 residues, located at the interface of thumb and palm sub-domains. The most complex architecture is of the fingers subdomain, as it is made up of two α-helices, six β-strands, and a zinc-binding loop that is indispensable for maintaining structural integrity [21][32]. An important flexible β-turn/loop, blocking/binding loop 2 (BL2 loop) that recognizes the P2-P4 of the LXGG motif of the substrate and closes upon binding of substrate/inhibitor, is located between β11–12 strands spanning the residues from 267–271, [26][32].

PLpro shares a strikingly similar USP fold like the cellular DUBs, with a structurally conserved active site fold and orientation of catalytic triad residues Cys-His-Asp/Asn. Previous studies have reported successful identification and repurposing of USP inhibitors against SARS-CoV and MERS [33][34][35]. These drugs effectively inhibited SARS-CoV after interacting with the residues of the substrate binding sites [34]. Therefore, repurposing USP inhibitors is an attractive alternative strategy that can assist in quickly identifying potentially effective molecules against SARS-CoV-2 PLpro due to the structurally conserved active site fold. Moreover, inhibitors with a cyanopyrrolidine warhead are reported to initiate a β-elimination reaction in the active site of USPs, resulting in irreversible inactivation of active site cysteine to dehydroalanine after desulfhydration reactions [36]. Cyanopyrrolidine forms a covalent enzyme-inhibitor complex in which the inhibitor can bind the active site of the enzyme and dissociate very slowly, which will result in prolonged inhibition of the enzymatic activity even after the free drug has been cleared off from the circulation [37]. Gliptins, a class of cyanopyrrolidine derivatives, are already in clinical use as an antidiabetic compound inhibiting dipeptidyl peptidase 4 (DPP4), a serine protease and a possible receptor for SARS-CoV-2 entry [37][38][39]. Notably, the DPP4 inhibitor, sitagliptin, is reported to exert an anti-inflammatory effect on the lungs by inhibiting the IL-1 and

IL-6 inflammatory pathways, eventually providing some relief against acute respiratory distress syndrome (ARDS) [40][41][42]. Repurposing gliptins and DUB inhibitors is hypothesized to serve a dual mode of action in inhibiting SARS-CoV-2; firstly by the possible inhibition of enzymatic activity of PLpro and secondly, via restoration of host innate immune responses [43].

The present study aims to identify and repurpose currently available DUB inhibitors and cyanopyrrolidine ring containing compounds against PLpro of SARS-CoV-2. This approach involves high-throughput structure-based virtual screening of an *in-house* library of compounds, consisting of DUB inhibitors and cyanopyrrolidine ring-containing compounds, against PLpro of SARS-CoV-2. High-throughput virtual screening and docking experiments predicted five of these compounds with docking scores comparable to known PLpro inhibitor, GRL0617, suggesting their potentiality as SARS-CoV-2 inhibitors. Of these, lithocholic acid, linagliptin, teneligliptin, and flupenthixol were able to significantly inhibit protease activity of PLpro as elucidated from FRET-based enzymatic assay and were able to display strong antiviral action in cell-based assays with half maximal effective concentration (EC_{50}) values in the range of 5-21 μM. In addition, crystal structure of PLpro and its complexes with inhibitory compounds have also been determined in this study that revealed unique binding allosteric sites and inhibitory mechanisms. To the best of our knowledge, this is the first study that opens a new approach of repurposing available DUB inhibitors and cyanopyrrolidine ring-containing compounds against PLpro of SARS-CoV-2.

MATERIAL AND METHODOLOGY

1. Hardware and software

MacOS Mojave workstation with an 8-core Intel Xeon E5 processor was used to perform all computational library screening and docking studies. LINUX workstation was used for carrying out all MD simulation studies, using GROMOS96 43a1 force field in GROMACS 5.1.1 suite. Other bioinformatics software, such as AutoDock 4.2.6 [44], PyMol [45], PyRx 0.8 [46], GROMACS 2019.5 [47], Open Babel [48], and online resources like Protein Data Bank (RCSB-PDB) [49], ESpript 3.0 [50], PDBeFold [51], NCBI, etc. were used in this study.

2. Structural comparison of PLpro and USP protein

Pairwise comparisons of secondary structure elements were performed with the web-based Secondary Structure Matching program (SSM), available within the Protein Data Bank (PDBeFold). For assessing structural similarities, crystal structures of SARS-CoV-2 PLpro (PDB ID: 6W9C), HAUSP/USP7 (PDB ID: 2F1Z), and USP2 (PDB ID: 5XU8) were downloaded from RCSB-PDB. The structures were fed into the PDBeFold-SSM portal and the hits from each pairwise comparison are ranked by their RMSD values, Q-score, and the number of aligned residues. The 3D alignment file was downloaded and analyzed in PyMol to observe conserved loops and residues. To gain more insights into the conserved residues at the substrate binding pockets (Ub/ISG15 binding site), multiple sequence alignment of SARS-

CoV-2 PLpro (PDB ID: 6W9C), HAUSP/USP7 (PDB ID: 2F1Z), and USP2 (PDB ID: 5XU8) was done using Clustal Omega/ESPript 3.0.

3. Structure-based screening of *in-house* DUB inhibitor library

An *in-house* library of ~81 compounds containing previously reported DUBs inhibitors and cyanopyrrolidine ring compounds was prepared, and screened against PLpro to identify potential antivirals against SARS-CoV-2. The SDF files for three-dimensional structures (3D) of all compounds were retrieved from PubChem (https://pubchem.ncbi.nlm.nih.gov/) database. 3D-crystal structure of PLpro of SARS-COV-2 (PDB ID: 6W9C) was retrieved from RCSB-PDB and prepared for virtual screening by removal of crystallographic water molecules and cognate ligand or ions from the protein. Using the automated function of AutoDock Vina, refinement of protein was done by addition of polar hydrogen atoms and the protein was saved in PDBQT format for further docking studies.

Before performing structure-based virtual screening, all the ligands were energy minimized by Universal Force Field (UFF) using Open Babel in PyRx 0.8. SDF files of all ligands were converted into PDBQT format for virtual screening against PLpro using an in-built Open Babel and AutoDock Vina module of PyRx 0.8. The grid centers for docking search space were set as X= -34.15, Y= 20.39, and Z=33.83, and the dimensions (Å) for X, Y, and Z axis were set as 36.46, 27.89, and 31.02 respectively. The size of the grid box was set centering on the substrate binding site for PLpro with a default exhaustiveness value of 8 for all ligands. A total of 9 different poses were generated for each ligand. Visual examination of the docked complexes possessing the highest binding affinities was carried out using PyMol for analyzing hydrogen and hydrophobic interactions. The top-ranked compounds possessing highest binding affinities and displaying key interactions with the targeted site were selected.

4. Molecular docking and simulation studies

Molecular docking of the top-hit ligands with PLpro of SARS-CoV-2 was carried out using AutoDock 4.2.6. Crystal structure of PLpro of SARS-CoV-2 (PDB ID: 6W9C) was downloaded from PDB and the PDBQT file of this energy minimized structure was used. AutoDock and AutoGrid tools available with AutoDock4 were used to calculate grid maps for pre-calculation of interaction energies of all interacting atoms. The center points were set as X= -34.430, Y= 27.180, and Z= 33.900; grid box dimensions were 100 Å ×100 Å×100 Å. Lamarckian genetic algorithm (GA) with a combination of maximum grid-based energy evaluation method was used for docking studies. The program was run for a maximum number of 25 genetic algorithm runs. All other parameters were set as default. Commonly known PLpro inhibitor GRL0617 was used as a reference control. Out of all the possible poses generated, the pose showing maximum binding affinity, hydrogen, hydrophobic interactions, and lowest RMSD values were chosen for detailed visual analysis using LigPlot and PyMol. Top 20 ligands displaying interactions similar to GRL0617 for targeted site of PLpro, possessing high binding affinities, and low RMSD values (< 2 Å) were sorted out. Of these

hits, the compounds that were recently reported as SARS-CoV-2 inhibitors in other studies were excluded from further studies. The compounds were finally selected based on the stability and interactions with the signature catalytic triad residues and BL2 loop and were processed for MD simulation studies.

To gain a deeper understanding of the stability of protein-ligand docked complexes, MD simulation was carried out for the docked complexes using GROMACS 2019.5 package with a GROMOS96 43a1 force field in Gromacs 5.1.4 suite on Ubuntu-based LINUX workstation. For performing all MD simulations of protein-ligands, the topology files of selected ligands were generated using PRODRG. The protein-ligand complexes were solvated in a cubic box by the addition of water molecules and counterions for ensuring the neutrality of the system. To minimize the steric clashes, the steepest descent algorithm for 50,000 iteration steps was used to perform energy minimization. Two different system equilibration phases were carried out for 500,000 steps. The first phase of system equilibration was performed at a constant number of particles, volume, and temperature (NVT) at 300K with short range electrostatic cut-off of 1.2 nm and regulation of temperature was done by using the Berendsen temperature coupling method. The second phase involved a constant number of particles, pressure, and temperature (NPT) ensemble at 300 K, for each step of 2fs. Particle Mesh Ewald (PME) method with a Fourier grid spacing of 1.6 Å was employed for calculation of long-range electrostatics. Finally, the MD simulation was carried out for 50 ns with integration time frame steps of 2 fs. The Root Mean Square Deviation (RMSD) values were calculated for PLpro protein and for all protein-ligand complexes.

5. SARS-CoV-2 PLpro purification

DNA sequence encoding the PLpro of SARS-CoV-2 was codon optimized for bacterial expression. PCR amplification of the gene encoding PLpro was carried out using synthesized gene (Invitrogen, Thermo Fisher scientific) as the template. After restriction digestion, the gene was cloned into the Nde1 and Xho1 restriction sites of pET28c bacterial expression vector which expressed PLpro as a fusion construct with an N-terminal histidine tag. The resulting plasmid was transformed into competent DH5α cells. These transformed cells were grown on Luria–Bertani (LB) agar plates supplemented with 50 μg/mL kanamycin with incubation at 37 °C overnight. Several colonies were picked and grown in 10 mL LB broth containing 50 μg/mL of kanamycin. The plasmid was isolated using MiniPrep isolation kit (Qiagen, USA) and the cloned plasmid was confirmed for PLpro insert by PCR amplification, restriction digestion, and Sanger sequencing.

After confirmation by Sanger sequencing, the resulting construct (pET28c-PLpro) was transformed into expression host *Rosetta* (DE3; Novagen, USA) in LB broth medium at 37 °C until the OD_{600} reached 0.6. At this point, the expression of protease was induced using 0.5 mM isopropyl-β-d-1-thiogalactopyranoside (IPTG) along with the addition of 1mM $ZnCl_2$. The induced cells were grown overnight at 18 °C and 180 rpm in an incubator. Finally, the

cells were harvested by centrifugation (6000 rpm for 10 min at 4 °C) and were resuspended in lysis buffer (50 mM Tris-HCl, pH 8.5, 500 mM NaCl, and 5mM DTT). Cells were homogenized using French press (Constant Systems Ltd, Daventry, England) and the cellular debris was removed by centrifugation at 10000 rpm for 1.5 h at 4 °C. The clarified supernatant was loaded onto nickel-nitrilotriacetic acid (Ni-NTA) beads (Qiagen, USA) in a gravity flow column and flow-through was collected after incubation for 30 min at 4 °C. After washing the resin with binding buffer (50 mM Tris-HCl, pH 8.5, 500 mM NaCl, and 5mM DTT), the recombinant PLpro protein was eluted with 100-500 mM imidazole in binding buffer. The eluted fractions were analyzed using 15% sodium dodecyl sulphate-polyacrylamide gel electrophoresis (SDS-PAGE). The fractions containing pure PLpro protein were pooled together and dialyzed against buffer containing 20 mM Tris-HCl, pH 8.5, 200 mM NaCl, and 5mM DTT. The dialyzed protein was concentrated using Amicon centrifugal filters (Millipore, Burlington, MA, USA) with a molecular weight cutoff of 10 kDa. The concentration of purified PLpro was determined by using the Bradford Assay. Using the wild type PLpro plasmid as the template, site directed mutagenesis (C111S) was performed by an overlapping PCR strategy using synthetic primers. Expression and purification of C111S mutant was performed using the same protocol as that for the wild type enzyme.

6. SARS-CoV-2 PLpro protease inhibition assay

To characterize *in vitro* enzymatic activity of SARS-CoV-2 PLpro and to assess the inhibitory potential of identified compounds, a high-throughput fluorescence resonance energy transfer (FRET) based enzymatic assay was developed as described previously [9]. To carry this out, a commercially available fluorogenic substrate Z-Arg-Leu-Arg-Gly-Gly-7-amido-4-methylcoumarin (Z-RLRGG-AMC) (Biolinkk, India) representing the C-terminal residues of ubiquitin was used. The experiment was carried out in 96-well non-binding black plates (Corning) in reaction buffer containing 50 mM HEPES (pH 7.5). The protease diluted in reaction buffer was added to each well at a final concentration of 1 μM. Enzymatic reaction was initiated with the addition of fluorogenic substrate peptide at a concentration of 1.5 μM and the fluorescence signals were monitored continuously using a plate reader (Synergy HT, BioTek Instruments, Inc) with filters for excitation at 360/40 nm and emission at 460/40 nm for 30 min. PLpro C111S was used as a negative control to determine whether signal generation was dependent on proteolytic activity of enzyme. Data from duplicate set of readings was averaged together to plot a graph for relative fluorescence and time.

To assess the inhibitory potential of screened compounds, the assay was assembled as follows: 1 μM PLpro in 50 mM HEPES buffer was incubated with increased concentration of compounds (Cayman chemicals, USA) ranging from 0.1 μM to 500 μM and was dispensed into wells of 96-well plate. Reactions were initiated with 1.5 μM of fluorogenic substrate peptide and the fluorescence signals were monitored continuously for 10 min at excitation wavelength of 360/40 nm and emission wavelength of 460/40 nm. Data from duplicate set of readings were averaged together and a graph for percentage inhibition vs concentration was

plotted for each selected compound after non-linear curve fitting using GraphPad Prism. Concentration of inhibitor that resulted in 50% inhibition (IC_{50}) was calculated.

7. **Binding kinetic analysis using Surface Plasmon Resonance (SPR)**
The binding kinetics and affinity of identified compounds to PLpro of SARS-CoV-2 were analyzed by SPR using a Biacore T200 system (GE Healthcare) at 25 ˚C. In brief, histidine-tagged PLpro was diluted to 10 μM concentration at pH 7.3 and was then captured on NTA chip in 1X Phosphate buffer saline (1X PBS) running buffer (137 mM NaCl, 2.7 mM KCl, 10 mM Na_2HPO_4, and 1.8 mM KH_2PO_4) degassed and filtered through 0.22 μM membrane filter. The binding kinetic studies were performed by collecting the data at 25°C by injecting the concentration series of analyte over the surface of chip having the immobilized PLpro with the following injection parameters: 10μL/min flow rate and 60 s association and dissociation phases. The surface was regenerated after each dissociation phase. Equilibrium dissociation constants (K_D) of each pair of PLpro-ligand interaction were calculated using Biacore Evaluation Software (GE Healthcare) by fitting to a 1:1 Langmuir binding model.

8. **Virus propagation and cells**
The wild type SARSCoV-2/Human/IND/CAD1339/2020 strain was isolated from laboratory confirmed COVID-19 patients in India. After genetic characterization by whole genome sequencing (GenBank accession no: MZ203529), the virus was passaged in Vero cells and supernatant was collected and clarified by centrifugation before being aliquoted for storage at −80 °C [52]. Virus titer was measured in Vero cells by TCID50 assay. Vero cell line used in this study were procured from NCCS (Pune, India). Cells were maintained in high glucose Dulbecco's-modified essential media (DMEM; HiMedia, India) augmented with 10% heat inactivated fetal bovine serum (FBS; Gibco, USA), 100 units of penicillin, and 100 mg streptomycin/mL. Assessment of cytotoxic effect and the inhibitory potential of identified compounds against SARS-CoV-2 replication was carried out in Vero cells. All procedures related to virus culture were handled in Biosafety level 3 facility at Indian Veterinary Research Institute (IVRI), Izatnagar, Bareilly, following standard WHO guidelines.

9. **Viral load reduction assay:** To determine the cytotoxic profiles of identified compounds on Vero cells, MTT assay was performed as described previously [53]. Briefly, Vero cells were seeded onto wells of 96-well cell-culture plate at a density of 1×10^4 cells/well and the plates were incubated at 37 °C and 5% CO_2 overnight for proper adherence of cells. The culture media was removed and the monolayer of cells was treated with increased dilutions of compounds (1-100 μM) prepared in DMEM media in triplicates. Post incubation period of 48 h, the media was removed, 20 μl/well MTT [3-(4,5-dimethylthiazol-2-yl)-2,5-diphenyl tetrazolium bromide] solution (5 mg/mL) was added and incubated for 4 h at 37 °C in a humidified incubator with 5% CO_2. Following this, the MTT solution was removed and the

formazan crystals were dissolved in DMSO. Absorbance was measured at a wavelength of 550 nm using a multimode plate reader (Synergy HT, BioTek Instruments, Inc). Results were expressed as percentage viability of cells in comparison to untreated cell control. Percentage viability for each compound was calculated and a dose-response curve was plotted using GraphPad Prism software.

Viral load reduction assay was performed by quantitative reverse transcription-polymerase chain reaction (qRT-PCR). Briefly, Vero cells were seeded and cultured in 24-well plate in DMEM media supplemented with 10% FBS and 100 units of penicillin and 100 mg streptomycin/mL, at 37 °C and 5% CO_2. Three hours before infection, the cells were washed with PBS and the media was replaced with DMEM (2% FBS) containing gradient of diluted experimental compounds. Post incubation, the cells were washed with PBS and were infected with SARS-CoV-2 at a Multiplicity of infection (MOI) of 0.01 in media without FBS and again incubated for 1.5 h. After incubation, the viral inoculum was removed and the cells were washed with PBS and then replenished with fresh medium containing dilutions of compounds. Plates were then incubated for 48 h at 37 °C and 5% CO_2. At 48 hours post infection (hpi) the plates were freezed at -80ºC. On the following day plate was thawed, and viral RNA was extracted from cell lysate of SARS-CoV-2 infected cells using HiPurA™ Viral RNA Purification Kit, according to the manufacturer's instructions. One-step qRT-PCR was performed with primers targeting the SARS-CoV-2 envelope (E-gene) and RdRP region using the commercially available COVISure-COVID-19 Real-Time PCR kit (Genetix), as per the manufacturer's instructions, to quantify the virus yield. The thermocycling conditions consist of 15 min at 50 °C for reverse transcription, 95 °C for 2 min, followed by 40 cycles of 30 s at 95 °C and 30 s at 60 °C. All experiments were performed in duplicates. Percentage inhibition was calculated based on ΔΔCt. The percentage inhibition versus concentration graph was plotted to calculate the EC_{50} values using the linear regression.

10. **Viral Titer by TCID50 (Median Tissue Culture Infectious Dose) assay:** Infectious virus production by compound treated and infected cells as compared to only infected cells was evaluated by the standard 50% tissue culture infectious dose ($TCID_{50}$) and was expressed as $TCID_{50}$/mL. For this purpose, 4×10^4 Vero cells/well were seeded in a 96-well plate and the plate was incubated at 37 °C and 5 % CO_2, till confluency. The freeze-thawed cell lysate of cells infected and treated with different concentrations of compounds collected at 48 hpi of the antiviral assay was subjected to 10-fold serial dilutions (10^1 to 10^8). Compound untreated and infected samples were used as positive control, and samples with only cell-culture media were used as a negative control. These dilutions were inoculated on Vero cells. Cells were incubated for 3 to 4 days at 37 °C and 5 % CO_2. [54]. The plate was monitored daily for the appearance of a cytopathic effect (CPE). Post incubation, the viral inoculum was removed, and 10% formaldehyde (in PBS) was used to fix cells for 2 h at room temperature, followed by staining with 0.5% crystal violet solution for 1 h. Percent infected dilutions immediately

above and immediately below 50% were determined. $TCID_{50}$ was calculated on the basis of Reed and Muench method.

11. **Crystallization of ligand free PLpro and its complex with identified compounds:** Crystallization experiments for C111S PLpro mutant were performed using sitting-drop vapor diffusion method. To achieve this, the purified protein was concentrated for crystallization and crystal tray was set up with protein:reservoir ratio of 1:1, 2:1, and 1:2 with reservoir buffer containing crystallization condition [0.1 M Tris-HCl (pH 7.5-9.0), 1.4 M NaH_2PO_4, and 2-15% Glycerol] in 96-well sitting-drop plate (Corning, USA). The protein drops were equilibrated in sitting drop setup with 100 µL reservoir solution and the plate was incubated at 4℃ or 20℃. The crystals were manually harvested from the drop and were cryo-protected by reservoir well solution plus 20% ethylene glycol and snap-frozen in liquid nitrogen for diffraction data collection. PLproC111S-inhibitor complex crystals were obtained by soaking $PLpro^{C111S}$ crystals with inhibitor powder for 30 min and cryoprotected in reservoir liquor supplemented with 20% glycerol.

12. **X-Ray data collection, structure determination and refinement:** Diffraction data for C111S PLpro and its complex with identified compounds was collected at the Home Source, Macromolecular crystallography Unit, IIC, IIT Roorkee. Datasets were processed using Aimless module of CCP4i2 and the structures were solved by molecular replacement. The search model was C111S PLpro structure (PDB: 6WRH). Model for SARS-CoV-2 C111S PLpro and its complex with selected compounds was subjected to iterative rounds of model building using COOT and refinement of atomic coordinates and B-factors in refmac5 that allowed for the correct placement of sidechains and loops. Structural figures will be generated by software PyMol (Schrödinger, New York, NY, USA).

Result:

PLpro is a deubiquitinating and deISGylating enzyme: Structural studies have contributed to a detailed understanding of SARS-CoV-2 PLpro with other DUBs. Reminiscent of the overall architecture of DUBs of the USP family, PLpro shares a similar active site architecture with host USP7 (also known as HAUSP) and USP2 proteins, including the signature catalytic triad (Cys-His-Asp/Asn) at the interface of its thumb and palm domains. A detailed structural comparison of the PLpro with UPS7 and USP2 proteins was carried out using the PDBeFold (SSM: Secondary Structure Matching) and multiple sequence alignment was performed with ESPript3 **(Supplementary Figure 1)**. Although these proteins share a very low percentage of sequence identity with an alignment of only 187 residues of PLpro with USP7 and USP2 proteins, the structural superimposition topologies are reasonably similar with an overall RMSD value of 1.68Å and 1.24 Å for USP7 and USP2, respectively **(Figure 1).** Briefly, the palm subdomain of

PLpro, USP7, and USP2 comprises of 6 β-sheets and includes the conserved catalytic triad (Cys-His-Asp/Asn) of the active site. Beyond the catalytic residues, USPs contain N and C-terminal extensions that aid in substrate recognition and binding. The BL2 of SARS-CoV-2 PLpro (residues 267–272) that provides floor to ubiquitin tail, also superimposes well with the BL2 loops of USP7 and USP2 **(Figure 1)** [55][56]. Interestingly, the zinc-binding domain located in the thumb region of SARS-CoV-2 comprises of 4 cysteine residues (Cys189, Cys192, Cys224, and Cys226) and the same pattern is observed for USP2 as well (Cys334, Cys337, Cys381, and Cys384) [57]. Contrastingly, some of the four cysteine residues of this metal binding motif have been mutated during evolution in USP7 and other DUBs due to which the zinc binding ability was lost while the fold integrity was still retained [57]. Importantly, few residues of the substrate binding or proteolytic cleft formed near the BL2 loop occupying the S3/S4 pocket are also conserved. For instance, Gly 269, Gly 271, His 272, and Tyr 273 (numbering as per PLpro) are conserved between USP7 and USP2 signifying that the catalytic site and few adjacent residues are conserved **(Figure 1 and Supplementary figure 1)** [30][32]. Nevertheless, the structural architecture of the active/catalytic site is very similar in PLpro, USP7, and USP2, suggesting that at least some inhibitors may display cross activity among these proteases.

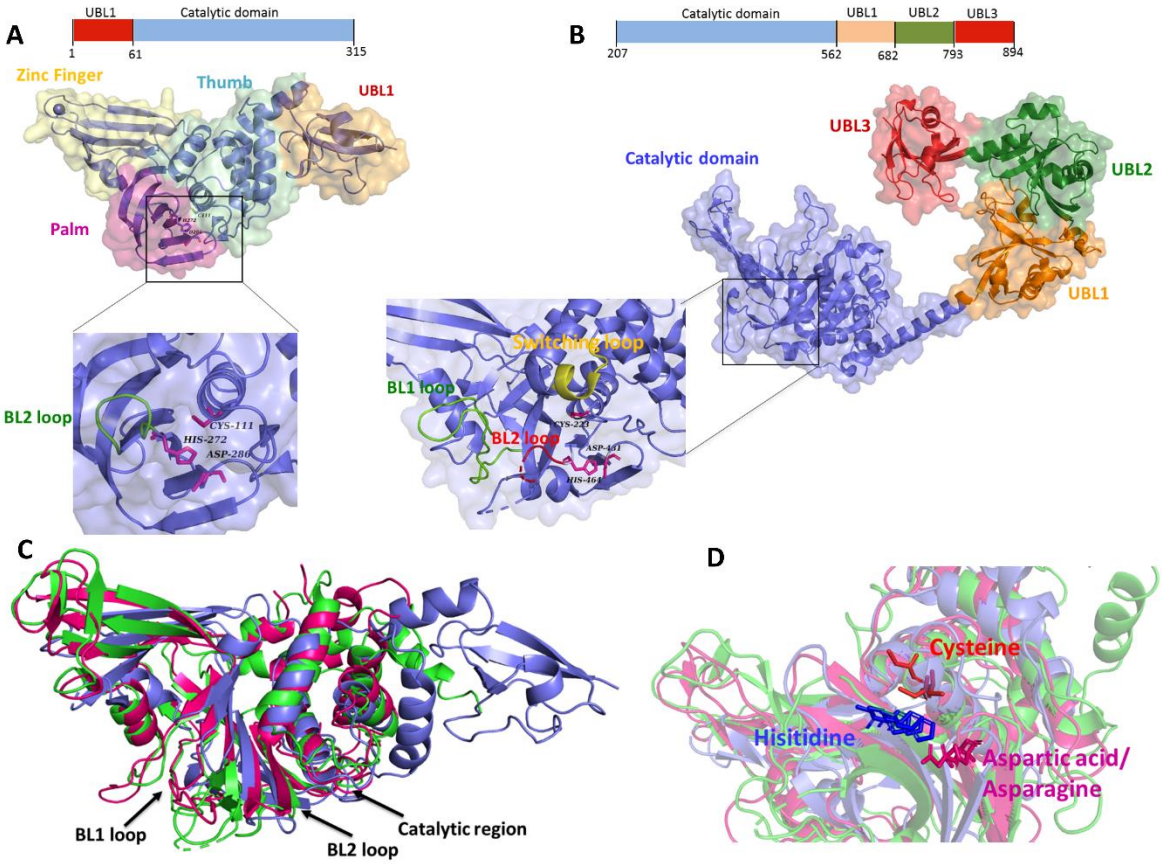

Figure 1: Domain organization and comparison of structural motifs of SARS-CoV-2 PLpro with cellular DUBs, USP2 and USP7 **A)** Surface view representation of overall structure of PLpro (PDB ID: 6W9C) with thumb (Blue), palm (Magenta), and Zinc-finger domains (Yellow). The catalytic triad residues of PLpro, Cys111, His272, and Asp286 are represented as magenta sticks in zoomed in view **B)** Surface representation of the domain organization and structural architecture of USP7 (PDB ID: 5FWI). The catalytic triad residues are marked as magenta sticks, UBL1 (Orange), UBL2 (Forest green), UBL3 (Red), Binding loop 1 (Green ribbon), Binding loop 2 (Red ribbon), and switching loop (Yellow ribbon). The positioning of catalytic triad residues is represented in magnified view. **C)** Structural superimposition of secondary structure elements of PLpro (Purple; PDB ID: 6W9C), USP7 (Green; PDB ID: 2F1Z), and USP2 (Magenta; PDB ID: 5XU8). A total of 187 residues of each protein chosen by web based server PDBeFold, were aligned based on the secondary structure elements. Cartoon representation shows PLpro in purple, USP2 in magenta, and USP7 in green **D)** Catalytic triad residues of PLpro, USP2, and USP7 represented in sticks, are completely superimposed Cys (red), His (blue), and Asp (magenta).

Structure-based identification of PLpro inhibitors

Crystal structure of PLpro in complex with GRL0617 inhibitor provides a basis for identifying potential inhibitors targeting the active site of SARS-CoV-2 PLpro [32]. To achieve this, an *in house* library of 81 compounds consisting of previously reported DUB inhibitors and cyanopyrrolidine ring-containing compounds, was subjected to high-throughput virtual screening protocol using an in-built AutoDock Vina module of PyRx 0.8 (**Supplementary Table 1**). A total of 20 compounds obtained after virtual screening were shortlisted based on binding affinities and RMSD values (<1 Å). The resulting scores of virtual screening for these 20 compounds are listed in **Table 1**. Among these top hits, the compound Pimozide, MF094, FT671, ML323, FT827, GNE6640, and N-cyanopyrrolidine screened and identified in our study, were also reported recently to inhibit proteolytic activity of PLpro of SARS-CoV-2, thereby validating this developed protocol [9][58]. Published literature highlights efficacy of sitagliptin and gemigliptin in type II diabetes mellitus patients infected with SARS-CoV-2 when administered as a montherapy or in form of a combination therapy [59][60]. A recent study highlighted significant inhibitory effect of sitagliptin against PLpro of SARS-CoV-2 [61]. These compounds were therefore omitted from further studies and the remaining compounds were processed to gain further insights into binding modes and stabilities of protein-ligand complexes. Based on binding energies, number of polar/hydrophobic interactions, and availability, a total of five compounds were processed for detailed re-docking and MD simulation followed by *in vitro* studies.

Table 1: List of top 20 hits identified after virtual screening of *in house* library along with binding energies.

Sr. No.	Name of compound	AutoDock Vina Binding energy (kcal/mol)
1	**Lithocholic acid hydroxyamide**	-8.3
2	**HBX28364**	-7.9
3	**Pimozide**	-7.8
4	**Lithocholic acid (LCAE)**	-7.6
5	**Gemigliptin**	-7.5
6	**Linagliptin**	-7.5
7	**MF094**	-7.5
8	**FT671**	-7.4
9	**ML323**	-7.4
10	**XL188**	-7.3
11	**Curcusone D**	-7.2
12	**N-cyanopyrrolidine**	-7.2
13	**Sitagliptin**	-7.2
14	**HY50736**	-7
15	**Denagliptin**	-6.9
16	**Flupenthixol**	-6.9
17	**FT827**	-6.9
18	**GNE 6640**	-6.9
19	**Teneligliptin**	-6.8
20	**Vildagliptin**	-6.4

Binding modes of inhibitors targeting PLpro of SARS-CoV-2:

Owing to the structural similarities in active site architecture of PLpro and DUB enzymes, USP2 and USP7, re-docking and simulation studies of selected 5 compounds were carried out using AutoDock4.2.6 and Gromacs. To examine the validity of the designed AutoDock parameters and our docking protocol, docking studies were executed with a previously described SARS-CoV-2 PLpro inhibitor, GRL0617. The same parameters were then used for re-docking studies of the selected compounds against the substrate binding site of PLpro. The predicted AutoDock binding affinities for these compounds were in the range of -6.9 kcal/mol to -8.1 kcal/mol (**Table 2**). While the docking score for the native ligand GRL0617 is − 6.94 kcal/mol. Superimposition of these inhibitors on PLpro-GRL0617 complex suggests that each of these 5 compounds occupied the same substrate binding cleft as occupied by the reference compound GRL0617 [32] (**Figure 2A**). The binding mode of GRL0617 with PLpro revealed an important hot-spot site covering the residues Leu162, Gly163, Asp164, Glu167, Met208, Pro247, Pro248, Tyr264,

Tyr268, Gln269, Gly271, and Tyr273, Thr301 that were targeted in this study for antiviral drug discovery [29][32] **(Figure 2A)**. Re-docking studies of flupenthixol revealed that the compound displays a high binding affinity of -8.11 kcal/mol and forms four hydrogen-bonds with active site residues Asp164, Arg166, Tyr273, and Asp302 (**Figure 2B and supplementary figure 2**). In addition, hydrophobic interactions between flupenthixol and PLpro complex (Pro248, Tyr264, Gly266, Asn267, Tyr268, Thr301) also contributed to stabilization of this protein-ligand complex (**Figure 2B**). Lithocholic acid is the second best candidate that interacts with three H-bonds with targeted amino acids Arg166 and Tyr268 along with ten hydrophobic interactions **(Figure 2C and Table 2)**. Similarly, vildagliptin also displayed a strong network of two H-bonds and ten hydrophobic interactions with the targeted site **(Figure 2D, supplementary figure 2, and Table 2)**. Like other top hits, teneligliptin and linagliptin also occupied catalytic groove of PLpro forming H-bonds with key GRL0617 binding residues (Asp164: teneligliptin; Glu167: linagliptin) (**Figure 2E and 2F**). The complexes of teneligliptin and linagliptin are further stabilized by extensive hydrophobic interactions primarily involving Leu162, Gly163, Pro248, Tyr264, Gly266, Asn267, and Tyr268 substrate binding residues of PLpro (**Figure 2E and 2F**). To further the stability of docked complexes, molecular dynamic simulation of the selected 5 compounds with PLpro was carried out for 50 ns (**Supplementary figure 3**). The overall ligand/protein complex showed no major differences in the overall stability as observed for only PLpro, with an average RMSD value in the range of 0.1-0.4 Å for all complexes (**Supplementary figure 3**). All complexes attained equilibrium after and were stable throughout the run. Collectively, the data indicates that the selected compounds are valid starting points for optimization and development of new inhibitors against SARS-CoV-2.

Table 2: Promising antivirals for PLpro of SARS-CoV-2 obtained after detailed molecular docking and MD simulation studies. Binding energies, chemical structures, polar, and hydrophobic interactions are tabulated.

Sr. No.	Name of compound	AutoDock Binding energies	Hydrogen bonds		Hydrophobic interactions
			Bonds (lig - protein)	Bond length (Å)	
1	**Flupenthixol** 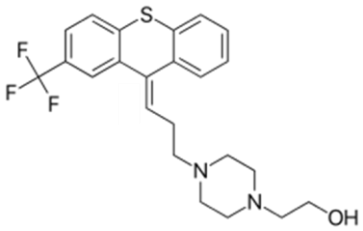	**-8.11**	O-OD1 (Asp164)	3.17	Pro248, Tyr264, Gly266, Asn267, Tyr268, and Thr301
			O-N (Arg166)	3.16	
			O-OH (Tyr273)	2.95	
			O-OD2 (Asp302)	2.71	

2	**Lithocholic acid (LCAE)** 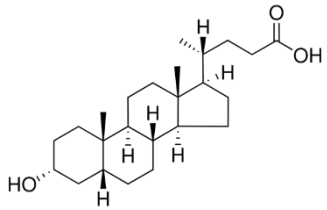	**-7.54**	O4-NE & O3-NH2 (Arg166)	2.87 and 3.05	Leu162, Gly163, Asp164, Met208, Ser245, Ala246, Pro248, Tyr264, Tyr273, and Thr301
			O2-O (Tyr268)	2.80	
3	**Vildagliptin** 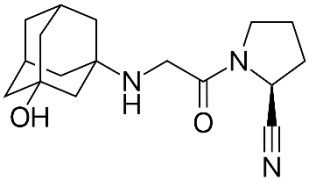	**-7.41**	O4-O (Gly163)	2.55	Leu162, Asp164, Arg166, Met208, Ala246, Pro247, Pro248, Tyr264, and Thr301
			N1-OH and O2-OH (Tyr273)	3.19 and 3.09	
4	**Teneligliptin** 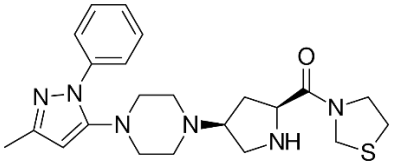	**-7.29**	N3 – OD1 (Asp 164)	2.41	Leu162, Gly163, Pro248, Tyr264, Gly266, Asn267, and Tyr268
			N3-OH (Tyr 273)	2.78	
5	**Linagliptin** 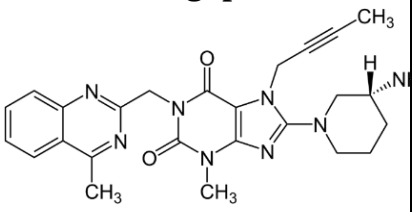	**-6.98**	N27-OE1 (Glu167)	3.11	Leu162, Gly163, Asp164, Pro248, Tyr264, Gly266, Asn267, Tyr268, Tyr273, and Thr301

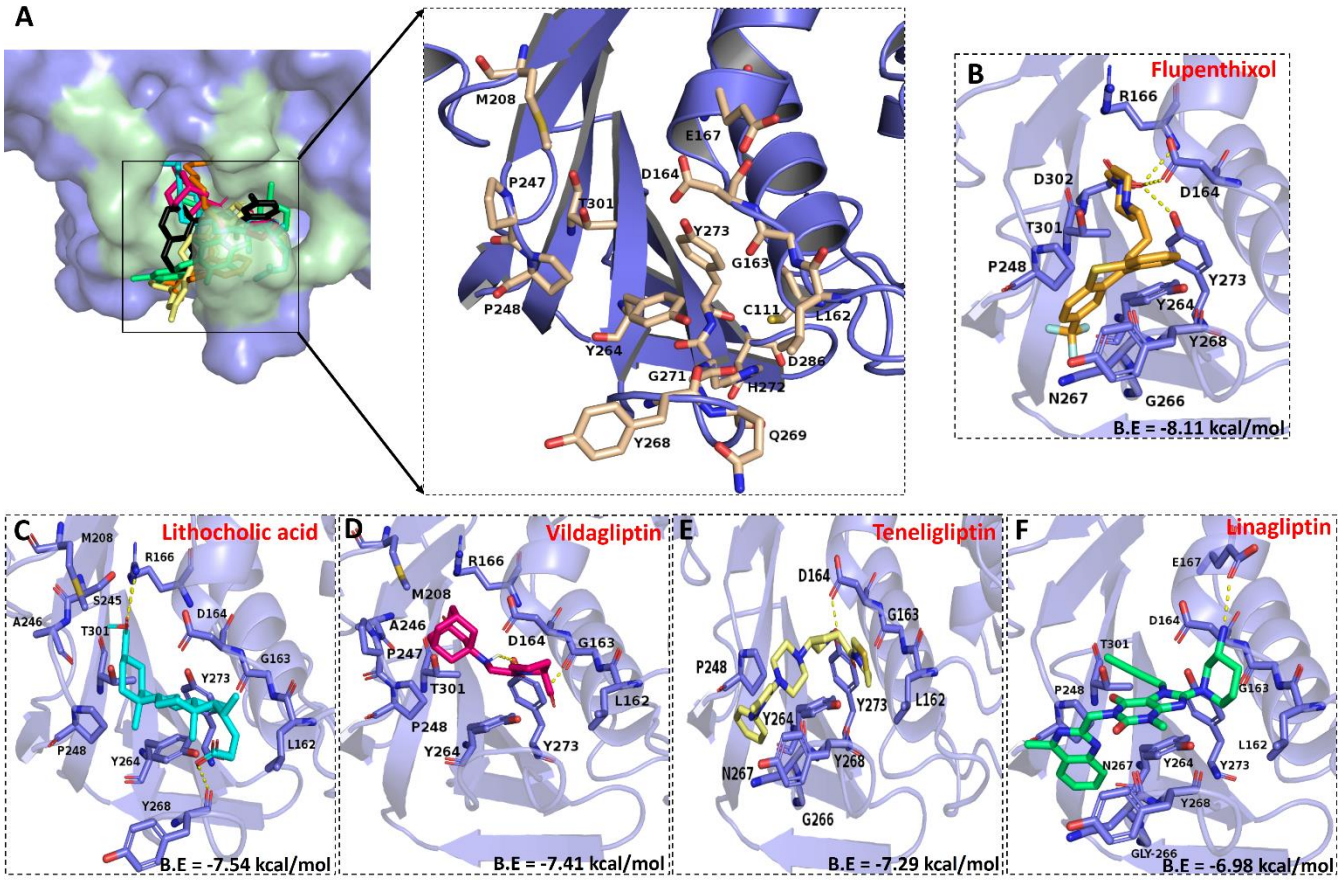

Figure 2: Docking of PLpro inhibitors: A) 3D interactions of SARS-CoV-2 PLpro in complex with DUBs inhibitors. The residues of substrate binding cleft and the BL2 loop near the active site is indicated. Co-crystallographic pose of GRL0617 (PDB ID: 6W9C) superimposed with the predicted binding modes of identified compounds in the active site of PLpro is depicted. Cartoon representation for network of contacts between PLpro (slate blue) and the selected inhibitors **B)** Flupenthixol (orange stick), **C)** Lithocholic acid (cyan stick), **D)** Vildagliptin (Pink stick), **E)** Teneligliptin (yellow stick), and **F)** Linagliptin (green stick). Residues of PLpro that are predicted to interact with the inhibitor are shown with the stick models. Hydrogen bonds are indicated by yellow dashed lines.

Inhibitory effect of compounds on proteolytic activity of SARS-CoV-2 PLpro:

Having established the enzymatic assay for proteolytic activity of PLpro, the inhibitory potential of five compounds selected from virtual screening and docking studies was quantified. To achieve this, recombinant SARS-CoV-2 PLpro was expressed in Rosetta DE3 and subsequently purified using affinity chromatography. A single band at ~36kDa in SDS-PAGE signified pure PLpro protein **(Supplementary figure 4)**. Proteolytic activity of recombinantly purified PLpro was assessed by the optimized FRET-based protease assay, using the commercially available Z-RLRGG-AMC fluorogenic substrate representing the C-terminal residues of ubiquitin, as

described in methodology section. Purified PLpro C111S mutant was used as a negative control to conclude that the production of fluorescence signal generation was exclusively dependent on proteolytic activity of enzyme (**Supplementary figure 4**). The same FRET assay was used to assess and validate the inhibitory potential of the identified compounds, flupenthixol, lithocholic acid, vildagliptin, teneligliptin, and linagliptin against the enzymatic activity of PLpro. Among these selected compounds, both lithocholic acid and linagliptin robustly inhibited proteolytic activity of PLpro with over 80% inhibition of SARS-CoV-2 PLpro and half-maximal inhibitory concentration (IC_{50}) values of 27.5 ± 2.20 μM and 53.1 ± 0.01 μM, respectively (**Figure 3A and 3B**). The compounds flupenthixol and teneligliptin showed IC_{50} values of 53.5 ± 4.09 μM and 259.2 ± 0.72 μM (**Figure 3C and D**). In contrast to it, vildagliptin was not observed to show any significant inhibition with a maximum inhibitory effect of less than 50 percent only (IC_{50} > 500 μM) (**Figure 3E**). Owing to its low inhibitory potential, vildagliptin was not selected for SPR-based binding kinetic assays and cell-based studies against SARS-CoV-2. Considering the inhibitory potential of the selected four compounds, these primary hits were subjected to a series of SPR-based assays and cell-based studies.

Binding kinetic studies for PLpro inhibitors: To examine the binding kinetics and affinity of compounds against PLpro, SPR-based studies were performed. After immobilization of histidine-tagged PLpro on NTA chip, serial dose of selected compounds was allowed to flow over the chip and the time dependent optical signal was recorded. Consistent with the results of FRET assay, a dose-dependent increase in response was observed for binding of lithocholic acid, linagliptin, and flupenthixol to SARS-CoV-2 PLpro. As represented in **figure 3F**, the K_D values determined by SPR measurements for lithocholic acid-PLpro, linagliptin-PLpro, and flupenthixol-PLpro are 79.3 μM, 72.6 μM, and 258.1 μM, respectively. SPR data suggested that lithocholic acid and linagliptin bind to PLpro with stronger affinity in comparison flupenthixol (**Figure 3F**). While fitting the data for Teneligliptin, the derivatives of the binding response and the dissociation were nonlinear and attempts to fit the data with 1:1 Langmuir Binding model failed with teneligliptin (data not shown). Together with results of fluorescence assay, SPR data confirms that these top-hits can be taken up for cell-based *in vitro* studies.

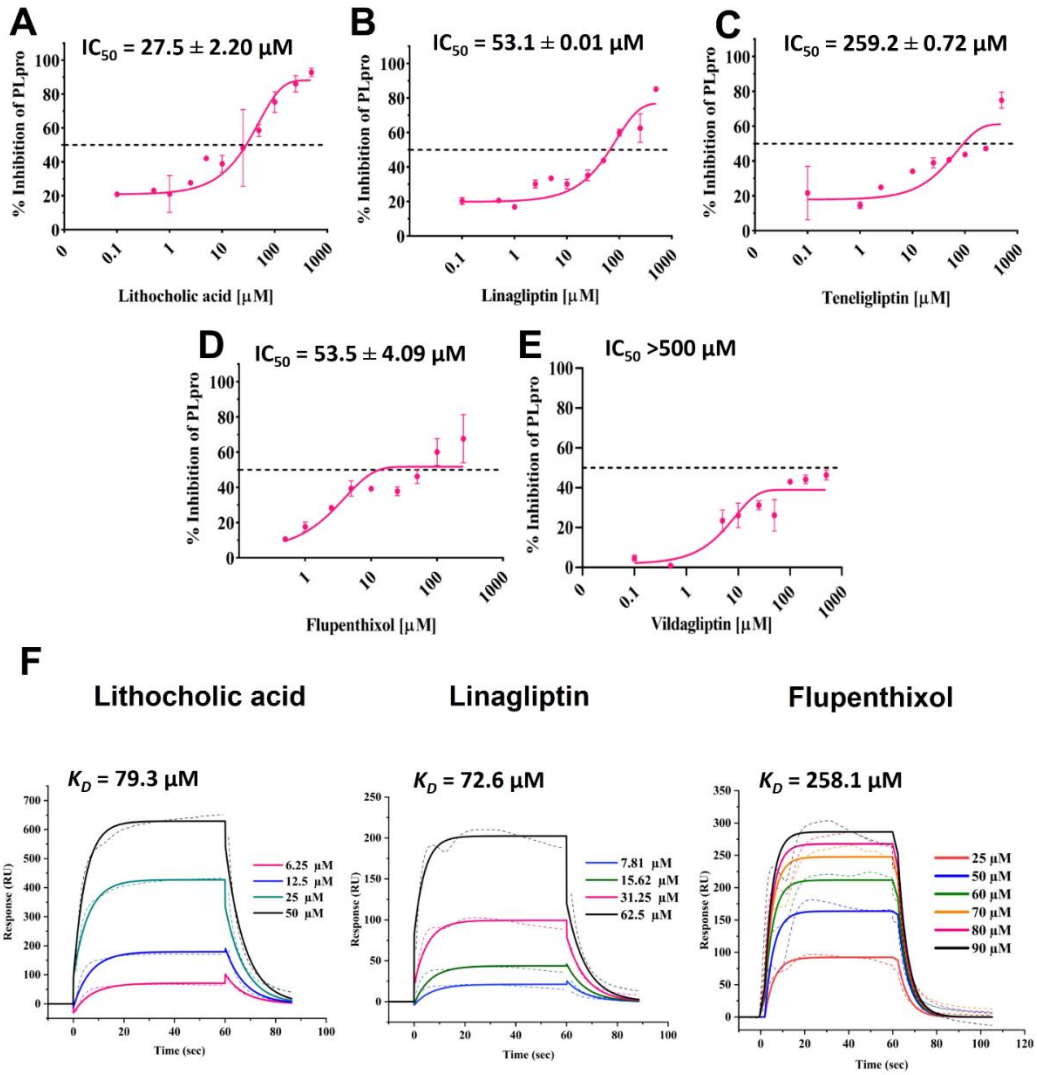

Figure 3: Inhibition of proteolytic activity of PLpro by selected compounds. The inhibitory potential of identified compounds **A)** Lithocholic acid, **B)** Linagliptin, **C)** Teneligliptin, **D)** Flupenthixol, and **E)** Vildagliptin against PLpro were tested using fluorogenic peptide Z-RLRGG-AMC as the substrate. Black dotted lines indicates the concentration of compound needed to inhibit the proteolytic activity of PLpro by half (IC_{50}). All data are shown as mean ± SEM, n = 2 independent experiments **F)** Evaluation of binding affinities of lithocholic acid, linagliptin, and flupentixol to SARS-CoV-2 PLpro using SPR. Sensorgrams elucidating the binding kinetics of selected analytes injected successively at increased concentrations against immobilized SARS-CoV-2 PLpro. The data was fitted using 1:1 Langmuir binding model. The processed sensograms are color coded, and the binding response is increasing with the increase in the concentration of the analyte. All experiments were conducted in duplicates. K_D, dissociation constant; RU, response units.

PLpro inhibitors restricts replication of SARS-CoV-2 *in vitro*

To ascertain whether the selected compounds were cytotoxic or not uninfected Vero cells were incubated with increased concentration of compounds and the cytotoxicity was measured using colorimetric MTT assay. As represented in **Figure 4**, lithocholic acid, linagliptin, and teneligliptin exerted very less cytotoxicity for Vero cells when tested across the range of concentrations (1-100 μM) and their calculated CC_{50} values were more than 100 μM (**Figure 4**). Contrastingly, flupenthixol displayed slight cytotoxicity at concentrations above 50 μM (**Figure 4**). The data suggests safe cytotoxic profile of the selected compounds and qualifies them for evaluation of antiviral potency against SARS-CoV-2.

After prioritizing the compounds on the basis of their inhibitory activity against the target protease combined with their low cellular toxicity, we next investigated their *in vitro* efficacy against clinical isolate of SARS-CoV-2 in Vero cells. Cells were pretreated with increased concentrations of compounds (lithocholic acid, linagliptin, teneligliptin and flupentixol) and were infected with SARS-CoV-2 at 0.01 MOI, followed by further incubation in medium with compound. Quantification of inhibition in viral replication was done by determining the percentage of positive infected cells in the presence and absence of the compound, at the end of the incubation period. To quantify this, cell lysate of treated and non-treated infected Vero cells was harvested to determine the viral load by quantifying the levels of viral RNA by real-time quantitative PCR (qRT-PCR) targeting the RNA-dependent RNA polymerase (RdRp) and N-protein. Consistent with the results of biophysical studies, lithocholic acid and linagliptin effectively inhibits replication of SARS-CoV-2 in Vero cells, exhibiting an EC_{50} value of 21 μM and 14.65 μM, respectively (**Figure 4A and 4D**). Surprisingly, Flupenthixol, which was observed to be a relatively weak inhibitor of enzymatic activity of PLpro, also displayed a strong inhibitory effect against SARS-CoV-2 at its non-toxic concentrations with an EC_{50} value of 5.10 μM (**Figure 4C**). Teneligliptin which was relatively a promising inhibitor based on PLpro enzymatic assay also inhibited SARS-CoV-2 infection in Vero cells at low micromolar range (EC_{50} = 20.82 μM) (**Figure 4B**).

To validate the results obtained from qRT-PCR, $TCID_{50}$ based studies were carried out. The effect of compounds on cells infected with SARS-CoV-2 was assessed by performing the virus titration. The sharp decrease in viral titer as compared to non-treated and virus infected positive control was observed in case of linagliptin (decrease of 4 log TCID50/ml) and teneligliptin (decrease of 2.5 log TCID50/mL) (**supplementary figure 5B and 5D**). Flupenthixol at the concentration of 20 μM, decreased the viral titer by 1.5 log TCID50/mL (**supplementary figure 5C**) and lithocholic acid (**supplementary figure 5A**) at its highest concentration of 50 μM reduced the titer by 1 log TCID50/mL as compared to virus control. We observed that treatment of cells with compounds involved in the present study, significantly reduced infectious virus production and apoptotic cell death associated with virus infection. A concentration-dependent decrease in virus titer was observed in the case of all compounds.

Together, the data suggest that these molecules displayed dose-dependent inhibition of replication of virus in Vero cells and hold considerable promise for therapeutics against SARS-CoV-2.

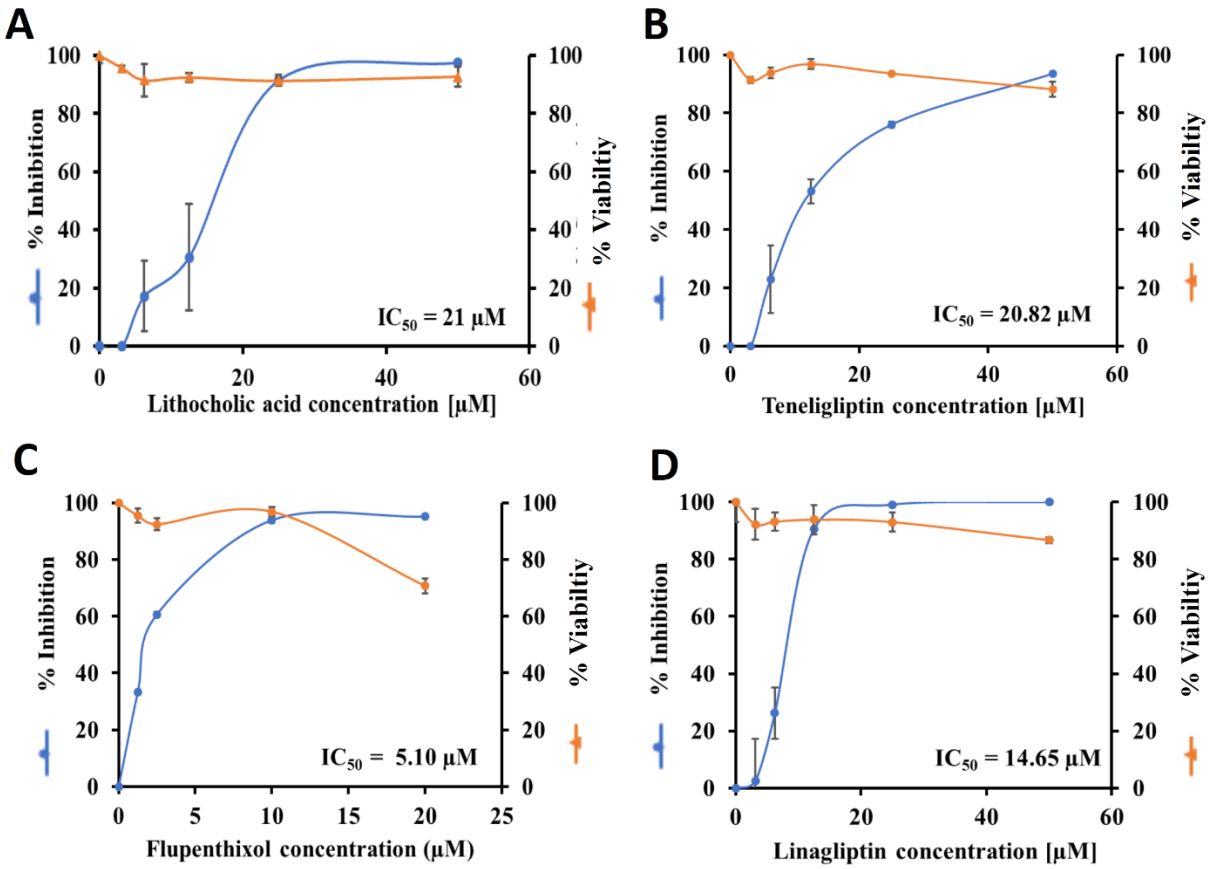

Figure 4: Comparative antiviral efficacy of selected compounds against SARS-CoV-2 infection *in vitro*. (A-D) Vero cells were treated with a series concentrations of indicated compounds **A)** lithocholic acid, **B)** linagliptin, **C)** flupenthixol, and **D)** teneligliptin and were then infected with SARS-CoV-2 at a multiplicity of infection (MOI) of 0.01. Cell culture supernatant was harvested and the inhibition pattern was quantified by qRT-PCR at 48 hpi. Graph represents percentage inhibition of SARS-CoV-2 replication. The experiments were repeated twice. The cytotoxicity of lithocholic acid, linagliptin, flupenthixol, and teneligliptin in Vero cells was determined by MTT assay. The left and right y-axis of each graph represents mean percent inhibition of virus yield and mean percent cell viability of the drugs, respectively. Representative data are shown from duplicate readings and the final graph was plotted for percentage viability of cells in the presence and absence of compounds (n = 2). Data represent mean ± SD.

Structure of PLpro in complex with identified compound: Protein structure for SARS-CoV-2 PLpro active site mutant C111S mutant was determined and refined to a resolution of 1.8 Å.

Data reduction was performed using Aimless module of CCP4i2 and the structure was solved by molecular replacement using SARS-CoV-2 C111S PLpro structure (PDB: 6WRH) as a search model. Crystals of SARS-CoV-2 were soaked with reservoir solution containing compound for 2 hr and the soaked crystals were harvested and cryo-cooled in liquid nitrogen for X-ray diffraction data collection. The electron density for the lithocholic acid, protein, solvent, and bound zinc ion is good and the data is in a phase of refinement.

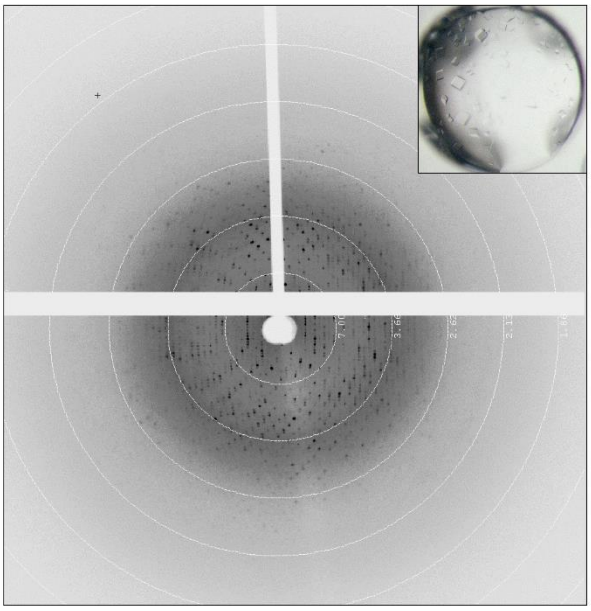

Figure 5: Crystallization and structure determination of PLpro-C111S in complex with inhibitor compound. Diffraction pattern of a PLproC111S-inhibitor crystal that shows sharp reflections extending to approximately 2.0 Å. Crystals of this quality were used to collect a data set by continuous rotation. Inset shows an example PLpro-C111S crystal.

Table 3: Comparison of enzymatic inhibition, SPR-binding kinetics, cytotoxicity, and antiviral activity of selected compounds.

Name of compound	IC_{50} (µM) values based on enzymatic assay	K_D values as determined by SPR	CC_{50} (µM)	EC_{50} (µM) values as per cell-based studies
Lithocholic acid	27.5 ± 2.20	79.3 µM	> 100	21
Linaglitpin	53.1 ± 0.01	72.6 µM		14.65
Teneligliptin	259.2 ± 0.72	Not determined		20.82
Flupenthixol	53.5 ± 4.09	258.1 µM	47 ± 1.86	5.10

Discussion:

The urgency of the COVID-19 pandemic and the recurring outbreaks by the variants of SARS-CoV-2 have heavily increased the challenges of curbing the pandemic of COVID-19. Therefore, there continues to be a need for preemptive strategies and drug modalities to treat COVID-19 and PLpro is considered a valuable target for it. Drug repurposing provides an alternative approach for quick identification of potential drugs to combat COVID-19, and targeting viral proteases offers additional advantages owing to their druggability and highly conserved substrate-binding pocket. Given that the substrate-binding pocket is highly similar among variants of SARS-CoV-2, the present study focused on identifying several bonafide inhibitors that might prove to be effective against different strains of SARS-CoV-2. In addition to the protease activity, PLpro possesses DUB and deISGylating activities as an evasion mechanism against the host antiviral immune response. Several host proteases, including USP2 and USP7 exhibit the same deconjugating activity and structural homology as host-encoded DUBs, marking their similarity as a noteworthy target to be explored.

Upon viral infection, type 1 interferons (IFN-α/β) produced by the immune cells of the host activate the production of ISG15. The upregulated ISG15 protein thereby conjugates with JAK, STAT, and IRF-3 through a process called ISGylation, all of which are key players of Type-1 elicited antiviral response of the host [62]. Activation of RIG-I-like receptors (RIG-I) and melanoma differentiation-associated protein 5 (MDA5) by ISGylation also leads to establishment of an antiviral state in host cell. To evade host immunity, PLpro antagonizes ISG15 dependent activation of MDA5 and RIG1 protein through its DUB activity [63]. A dysregulated interferon mediated antiviral response could lead to pro-inflammatory cytokine storm in the COVID-19 patients, a major cause of mortalities among infected patients [63]. Thus targeting PLpro might serve as a dual target that could avert SARS-CoV-2 infection either by inhibition of its proteolytic activity or by upregulation of innate immune response.

In light of previous studies, we sought to determine whether an inhibitor of DUBs could potentially be active against PLpro. For this purpose, a structural alignment of PLpro with USP2 and USP7 was done. The structural comparison revealed a very less percentage of conservation among the three selected DUBs. However, the structurally conserved active site fold and orientation of catalytic triad residues Cys-His-Asp/Asn provided a hint to repurpose available USP inhibitors against PLpro of SARS-CoV-2 (**Figure 1**). Encouraged by structural and functional similarities among these DUBs, an *in-house* library of DUB and cyanopyrrolidine-ring inhibitors was constituted. A total of five compounds were finally selected after comprehensive virtual screening, docking study, and MD simulation studies (**Table 2, Supplementary table 1, and Figure 2**). The enzymatic assays, SPR binding kinetic studies, and *in vitro* studies against SARS-CoV-2 show that lithocholic acid, linagliptin, teneligliptin, and flupentixol hold tremendous promise as a target to generate new class of antivirals against PLpro (**Figures 3 and 4**). Each of these compounds displayed biochemical inhibition of PLpro and also inhibited the virus and significantly reduced the infectious virus titer in cell-based assays (**Figures 3 and 4**). Concentration-dependent reduction in

viral copy number (**Figure 4**) and infectious viral titer (**supplementary figure 5**) well below their cytotoxic concentration highlights the effective anti-SARS-CoV-2 activity of compounds in the present study (**Table 3**). Interestingly, ligand-binding experiments using SPR were in line with the enzymatic inhibition and cell-based studies with observed K_D values in the micromolar range (lithocholic acid-PLpro: 79.3 μM; linagliptin-PLpro: 72.6 μM; flupenthixol-PLpro: 258.1 μM) (**Figures 3, 4, and 5**). Though teneligliptin failed to discern binding with PLpro in SPR assay, its antiviral data suggested significant inhibitory effect against SARS-CoV-2, proposing a hint for other possible off-targets that could be explored **(Figures 4 and supplementary figure 5)**. The superimposition of docked complexes of these identified compounds on PLpro demonstrated the occupancy of the same substrate-binding pocket and similar interactions with the active site as were reported for a small molecule inhibitor GRL0617 (**Figure 2**). The cytotoxicity profile in Vero cells showed a CC_{50} value of > 50 μM marking them safe for use (**Figure 4 and Table 3**).

Previous studies on lithocholic acid report it to be a potent inhibitor of intestinal inflammatory responses [64]. In another study, lithocholic acid is reported to exert antiviral action on replication of porcine delta coronavirus replication (PDCoV) [65]. Recent clinical and experimental data on COVID-19 provides evidence for reduced mortality in infected patients with or without type 2 diabetes, after the use of gliptins (e.g., sitagliptin, alogliptin, etc.). Gliptins, a class of DPP4 inhibitors, antagonize SARS-CoV-2 virulence either by enhancing GLP-1 anti-inflammatory activity or by reducing overproduction of cytokines and downregulating the activity of macrophages [66][67]. These classes of inhibitors may halt the disease progression to a hyperinflammatory state after viral infection [68]. Flupenthixol, an anti-depressant and antipsychotic drug, is reported to significantly inhibit the entry of SARS-CoV and MERS [69].

In conclusion, the compounds identified in this study offer new perspectives for treatment of COVID-19. However, the need for clinical studies cannot be ruled out to validate these *in vitro* findings. Because PLpro is a highly conserved protein among coronaviruses, these top leads appear as strong therapeutic candidates against the SARS-CoV-2 infection or its emerging variants.

Acknowledgement:

This research was funded by Science and Engineering Research Board, Department of Science & Technology, the Government of India (Proj. ref no. IPA/2020/000054). PK and ST thank Department of Biotechnology, Govt of India for supporting Bioinformatics Center at IIT Roorkee (reference number BT/PR40141/BTIS/137/16/2021). S.C. and A.K thank the Council of Scientific & Industrial Research (CSIR), Government of India for financial support. S.N. acknowledges the Ministry of Human Resource Development, (MHRD), and R.R thank University Grants Commission (UGC), Government of India for research fellowship. A.S thank Prime Minister's Research Fellows (PMRF), MHRD for research fellowship. The authors acknowledge and thank the Macromolecular Crystallographic Facility (MCU) at IIC, Indian Institute of Technology, Roorkee.

References:

[1] R. E. Baker, S. W. Park, C. E. Wagner, and C. J. E. Metcalf, "The limits of SARS-CoV-2 predictability," *Nat. Ecol. Evol.*, vol. 5, no. 8, pp. 1052–1054, 2021, doi: 10.1038/s41559-021-01514-z.

[2] R. Mudgal, S. Nehul, and S. Tomar, "Prospects for mucosal vaccine: shutting the door on SARS-CoV-2," *Hum. Vaccin. Immunother.*, vol. 16, no. 12, pp. 2921–2931, Dec. 2020, doi: 10.1080/21645515.2020.1805992.

[3] T. Crellen *et al.*, "Dynamics of SARS-CoV-2 with waning immunity in the UK population," *Philos. Trans. R. Soc. B Biol. Sci.*, vol. 376, no. 1829, p. 20200274, Jul. 2021, doi: 10.1098/rstb.2020.0274.

[4] E. Dolgin, "COVID vaccine immunity is waning-how much does that matter?," *Nature*, vol. 597, no. 7878, pp. 606–607, 2021.

[5] C. Giannitsarou, S. Kissler, and F. Toxvaerd, "Waning Immunity and the Second Wave: Some Projections for SARS-CoV-2," *Am. Econ. Rev. Insights*, vol. 3, no. 3, pp. 321–338, 2021, doi: 10.1257/aeri.20200343.

[6] W. F. Garcia-Beltran *et al.*, "Multiple SARS-CoV-2 variants escape neutralization by vaccine-induced humoral immunity," *Cell*, vol. 184, no. 9, pp. 2372-2383.e9, 2021, doi: https://doi.org/10.1016/j.cell.2021.03.013.

[7] Y. Weisblum *et al.*, "Escape from neutralizing antibodies by SARS-CoV-2 spike protein variants," *Elife*, vol. 9, Oct. 2020, doi: 10.7554/eLife.61312.

[8] A. Dubey, S. Choudhary, P. Kumar, and S. Tomar, "Emerging SARS-CoV-2 Variants: Genetic Variability and Clinical Implications," *Curr. Microbiol.*, vol. 79, no. 1, p. 20, 2021, doi: 10.1007/s00284-021-02724-1.

[9] H. Shan *et al.*, "Development of potent and selective inhibitors targeting the papain-like protease of SARS-CoV-2," *Cell Chem. Biol.*, vol. 28, no. 6, pp. 855-865.e9, 2021, doi: https://doi.org/10.1016/j.chembiol.2021.04.020.

[10] G. Li and E. De Clercq, "Therapeutic options for the 2019 novel coronavirus (2019-nCoV)," *Nat. Rev. Drug Discov. 2021 193*, vol. 19, no. 3, pp. 149–150, Feb. 2020, doi: 10.1038/d41573-020-00016-0.

[11] R. Rani *et al.*, "Multi-target direct-acting SARS-CoV-2 antivirals against the nucleotide-binding pockets of virus-specific proteins," *Virology*, vol. 577, pp. 1–15, 2022, doi: 10.1016/j.virol.2022.08.008.

[12] R. Rani, A. Singh, A. Pareek, and S. Tomar, "In silico guided drug repurposing to combat SARS-CoV-2 by Targeting Mpro, the key virus specific protease," 2020.

[13] A. Schäfer *et al.*, "Therapeutic efficacy of an oral nucleoside analog of remdesivir against SARS-CoV-2 pathogenesis in mice," *bioRxiv Prepr. Serv. Biol.*, p. 2021.09.13.460111, Sep. 2021, doi: 10.1101/2021.09.13.460111.

[14] G. Kokic *et al.*, "Mechanism of SARS-CoV-2 polymerase stalling by remdesivir," *Nat. Commun.*, vol. 12, no. 1, p. 279, 2021, doi: 10.1038/s41467-020-20542-0.

[15] J. Qiao *et al.*, “SARS-CoV-2 M(pro) inhibitors with antiviral activity in a transgenic mouse model,” *Science*, vol. 371, no. 6536, pp. 1374–1378, Mar. 2021, doi: 10.1126/science.abf1611.

[16] L. Zhang *et al.*, “Crystal structure of SARS-CoV-2 main protease provides a basis for design of improved α-ketoamide inhibitors,” *Science (80-.).*, p. eabb3405, Mar. 2020, doi: 10.1126/science.abb3405.

[17] D. Wenhao *et al.*, “Structure-based design of antiviral drug candidates targeting the SARS-CoV-2 main protease,” *Science (80-.).*, vol. 368, no. 6497, pp. 1331–1335, Jun. 2020, doi: 10.1126/science.abb4489.

[18] C. Ma *et al.*, “Discovery of SARS-CoV-2 Papain-like Protease Inhibitors through a Combination of High-Throughput Screening and a FlipGFP-Based Reporter Assay,” *ACS Cent. Sci.*, vol. 7, no. 7, pp. 1245–1260, Jul. 2021, doi: 10.1021/acscentsci.1c00519.

[19] P. V’kovski, A. Kratzel, S. Steiner, H. Stalder, and V. Thiel, “Coronavirus biology and replication: implications for SARS-CoV-2,” *Nat. Rev. Microbiol.*, vol. 19, no. 3, pp. 155–170, 2021, doi: 10.1038/s41579-020-00468-6.

[20] R. Arya *et al.*, “Structural insights into SARS-CoV-2 proteins,” *J. Mol. Biol.*, vol. 433, no. 2, p. 166725, Jan. 2021, doi: 10.1016/j.jmb.2020.11.024.

[21] J. Osipiuk *et al.*, “Structure of papain-like protease from SARS-CoV-2 and its complexes with non-covalent inhibitors,” *Nat. Commun.*, vol. 12, no. 1, p. 743, 2021, doi: 10.1038/s41467-021-21060-3.

[22] P. Ren *et al.*, “A multi-targeting drug design strategy for identifying potent anti-SARS-CoV-2 inhibitors,” *Acta Pharmacol. Sin.*, 2021, doi: 10.1038/s41401-021-00668-7.

[23] W. J. P. and D. Blossom, “SARS-CoV-2 dependence on host pathways,” *Science (80-.).*, vol. 371, no. 6532, pp. 884–885, Feb. 2021, doi: 10.1126/science.abg6837.

[24] R. Wioletta *et al.*, “Activity profiling and crystal structures of inhibitor-bound SARS-CoV-2 papain-like protease: A framework for anti–COVID-19 drug design,” *Sci. Adv.*, vol. 6, no. 42, p. eabd4596, Oct. 2021, doi: 10.1126/sciadv.abd4596.

[25] E. Weglarz-Tomczak, J. M. Tomczak, M. Talma, M. Burda-Grabowska, M. Giurg, and S. Brul, “Identification of ebselen and its analogues as potent covalent inhibitors of papain-like protease from SARS-CoV-2,” *Sci. Rep.*, vol. 11, no. 1, p. 3640, 2021, doi: 10.1038/s41598-021-83229-6.

[26] D. Shin *et al.*, “Papain-like protease regulates SARS-CoV-2 viral spread and innate immunity,” *Nature*, vol. 587, no. 7835, pp. 657–662, 2020, doi: 10.1038/s41586-020-2601-5.

[27] C. B. McClain and N. Vabret, “SARS-CoV-2: the many pros of targeting PLpro,” *Signal Transduct. Target. Ther.*, vol. 5, no. 1, p. 223, 2020, doi: 10.1038/s41392-020-00335-z.

[28] Z. Shen *et al.*, “Potent, Novel SARS-CoV-2 PLpro Inhibitors Block Viral Replication in Monkey and Human Cell Cultures,” *bioRxiv*, p. 2021.02.13.431008, Jan. 2021, doi: 10.1101/2021.02.13.431008.

[29] Z. Fu *et al.*, “The complex structure of GRL0617 and SARS-CoV-2 PLpro reveals a hot spot for antiviral drug discovery,” *Nat. Commun.*, vol. 12, no. 1, p. 488, 2021, doi: 10.1038/s41467-020-20718-8.

[30] R. Kiira *et al.*, “A noncovalent class of papain-like protease/deubiquitinase inhibitors blocks SARS virus replication,” *Proc. Natl. Acad. Sci.*, vol. 105, no. 42, pp. 16119–16124, Oct. 2008,

doi: 10.1073/pnas.0805240105.

[31] T. Klemm *et al.*, "Mechanism and inhibition of the papain-like protease, PLpro, of SARS-CoV-2," *EMBO J.*, vol. 39, no. 18, p. e106275, Sep. 2020, doi: 10.15252/embj.2020106275.

[32] X. Gao *et al.*, "Crystal structure of SARS-CoV-2 papain-like protease," *Acta Pharm. Sin. B*, vol. 11, no. 1, pp. 237–245, 2021, doi: https://doi.org/10.1016/j.apsb.2020.08.014.

[33] C.-Y. Chou *et al.*, "Thiopurine analogues inhibit papain-like protease of severe acute respiratory syndrome coronavirus," *Biochem. Pharmacol.*, vol. 75, no. 8, pp. 1601–1609, 2008, doi: https://doi.org/10.1016/j.bcp.2008.01.005.

[34] X. Chen, C.-Y. Chou, and G.-G. Chang, "Thiopurine Analogue Inhibitors of Severe Acute Respiratory Syndrome-Coronavirus Papain-Like Protease, a Deubiquitinating and deISGylating Enzyme," *Antivir. Chem. Chemother.*, vol. 19, no. 4, pp. 151–156, Feb. 2009, doi: 10.1177/095632020901900402.

[35] K.-W. Cheng *et al.*, "Thiopurine analogs and mycophenolic acid synergistically inhibit the papain-like protease of Middle East respiratory syndrome coronavirus," *Antiviral Res.*, vol. 115, pp. 9–16, 2015, doi: https://doi.org/10.1016/j.antiviral.2014.12.011.

[36] C. Bashore *et al.*, "Cyanopyrrolidine Inhibitors of Ubiquitin Specific Protease 7 Mediate Desulfhydration of the Active-Site Cysteine," *ACS Chem. Biol.*, vol. 15, no. 6, pp. 1392–1400, Jun. 2020, doi: 10.1021/acschembio.0c00031.

[37] P. Jadav *et al.*, "Long-acting peptidomimetics based DPP-IV inhibitors," *Bioorg. Med. Chem. Lett.*, vol. 22, no. 10, pp. 3516–3521, 2012, doi: https://doi.org/10.1016/j.bmcl.2012.03.078.

[38] E. Z. Fisman and A. Tenenbaum, "Antidiabetic treatment with gliptins: focus on cardiovascular effects and outcomes," *Cardiovasc. Diabetol.*, vol. 14, no. 1, p. 129, 2015, doi: 10.1186/s12933-015-0294-0.

[39] D. Pitocco, L. Tartaglione, L. Viti, M. Di Leo, A. Pontecorvi, and S. Caputo, "SARS-CoV-2 and DPP4 inhibition: Is it time to pray for Janus Bifrons?," *Diabetes Res. Clin. Pract.*, vol. 163, p. 108162, May 2020, doi: 10.1016/j.diabres.2020.108162.

[40] Y. Yang, Z. Cai, and J. Zhang, "DPP-4 inhibitors may improve the mortality of coronavirus disease 2019: A meta-analysis," *PLoS One*, vol. 16, no. 5, p. e0251916, May 2021, [Online]. Available: https://doi.org/10.1371/journal.pone.0251916.

[41] T. Kawasaki, W. Chen, K. Tatsumi, and S. M. Dudek, "DPP4 Inhibition Attenuates LPS-Induced Lung Injury in Mice," in *B27. The evil that endothelial cells do: implications for pulmonary vascular disease*, American Thoracic Society, 2018, pp. A2892–A2892.

[42] I. Valencia, C. Peiró, Ó. Lorenzo, C. F. Sánchez-Ferrer, J. Eckel, and T. Romacho, "DPP4 and ACE2 in Diabetes and COVID-19: Therapeutic Targets for Cardiovascular Complications? ," *Frontiers in Pharmacology* , vol. 11. p. 1161, 2020, [Online]. Available: https://www.frontiersin.org/article/10.3389/fphar.2020.01161.

[43] Z. Zong, Z. Zhang, L. Wu, L. Zhang, and F. Zhou, "The Functional Deubiquitinating Enzymes in Control of Innate Antiviral Immunity," *Adv. Sci.*, vol. 8, no. 2, p. 2002484, Jan. 2021, doi: https://doi.org/10.1002/advs.202002484.

[44] O. Trott and A. J. Olson, "AutoDock Vina: improving the speed and accuracy of docking with a new scoring function, efficient optimization, and multithreading," *J. Comput. Chem.*, vol. 31, no. 2, pp. 455–461, Jan. 2010, doi: 10.1002/jcc.21334.

[45] Schrodinger LLC, "The PyMOL Molecular Graphics System, Version 1.8." 2015.

[46] S. Dallakyan and A. J. Olson, "Small-molecule library screening by docking with PyRx," *Methods Mol. Biol.*, vol. 1263, pp. 243–250, 2015, doi: 10.1007/978-1-4939-2269-7_19.

[47] S. Pronk *et al.*, "GROMACS 4.5: a high-throughput and highly parallel open source molecular simulation toolkit," *Bioinformatics*, vol. 29, no. 7, pp. 845–854, Feb. 2013, doi: 10.1093/bioinformatics/btt055.

[48] N. M. O'Boyle, M. Banck, C. A. James, C. Morley, T. Vandermeersch, and G. R. Hutchison, "Open Babel: An open chemical toolbox," *J. Cheminform.*, vol. 3, no. 1, p. 33, 2011, doi: 10.1186/1758-2946-3-33.

[49] H. M. Berman *et al.*, "The Protein Data Bank," *Nucleic Acids Res.*, vol. 28, no. 1, pp. 235–242, Jan. 2000, doi: 10.1093/nar/28.1.235.

[50] X. Robert and P. Gouet, "Deciphering key features in protein structures with the new ENDscript server," *Nucleic Acids Res.*, vol. 42, no. W1, pp. W320–W324, Jul. 2014, doi: 10.1093/nar/gku316.

[51] E. Krissinel and K. Henrick, "Secondary-structure matching (SSM), a new tool for fast protein structure alignment in three dimensions," *Acta Crystallogr. Sect. D Biol. Crystallogr.*, vol. 60, no. 12 I, pp. 2256–2268, Dec. 2004, doi: 10.1107/S0907444904026460.

[52] P. Dhaka, A. Singh, S. Choudhary, P. Kumar, G. K. Sharma, and S. Tomar, "Discovery of anti-SARS-CoV-2 molecules using structure-assisted repurposing approach targeting N-protein," *bioRxiv*, p. 2022.03.12.484092, Jan. 2022, doi: 10.1101/2022.03.12.484092.

[53] M. Rajat *et al.*, "Selective Estrogen Receptor Modulators Limit Alphavirus Infection by Targeting the Viral Capping Enzyme nsP1," *Antimicrob. Agents Chemother.*, vol. 66, no. 3, pp. e01943-21, Jun. 2022, doi: 10.1128/aac.01943-21.

[54] L. J. REED and H. MUENCH, "A SIMPLE METHOD OF ESTIMATING FIFTY PER CENT ENDPOINTS12," *Am. J. Epidemiol.*, vol. 27, no. 3, pp. 493–497, May 1938, doi: 10.1093/oxfordjournals.aje.a118408.

[55] A. Pozhidaeva *et al.*, "USP7-Specific Inhibitors Target and Modify the Enzyme's Active Site via Distinct Chemical Mechanisms," *Cell Chem. Biol.*, vol. 24, no. 12, pp. 1501-1512.e5, 2017, doi: https://doi.org/10.1016/j.chembiol.2017.09.004.

[56] I. E. Wertz and J. M. Murray, "Structurally-defined deubiquitinase inhibitors provide opportunities to investigate disease mechanisms," *Drug Discov. Today Technol.*, vol. 31, pp. 109–123, 2019, doi: https://doi.org/10.1016/j.ddtec.2019.02.003.

[57] M. Renatus *et al.*, "Structural Basis of Ubiquitin Recognition by the Deubiquitinating Protease USP2," *Structure*, vol. 14, no. 8, pp. 1293–1302, 2006, doi: https://doi.org/10.1016/j.str.2006.06.012.

[58] C.-C. Cho *et al.*, "Drug Repurposing for the SARS-CoV-2 Papain-Like Protease," *ChemMedChem*, vol. 17, no. 1, p. e202100455, Jan. 2022, doi: https://doi.org/10.1002/cmdc.202100455.

[59] N. A. Alhakamy *et al.*, "Evaluation of the Antiviral Activity of Sitagliptin-Glatiramer Acetate Nano-Conjugates against SARS-CoV-2 Virus," *Pharmaceuticals* , vol. 14, no. 3. 2021, doi: 10.3390/ph14030178.

[60] M. Hazra, “Anti-Diabetic Prescriptions Evaluation for Metformin, Sitagliptin and Gemigliptin among Early Moderate Grade New Type II Diabetes Mellitus Patients in Global Tertiary Care Hospitals: An Analytical Study in Rational Pharmacotherapeutics,” *Journal of Basic and Clinical Pharmacy*, 2021. .

[61] A. Narayanan *et al.*, “Identification of SARS-CoV-2 inhibitors targeting Mpro and PLpro using in-cell-protease assay,” *Commun. Biol.*, vol. 5, no. 1, p. 169, 2022, doi: 10.1038/s42003-022-03090-9.

[62] D. S. M. Lewis *et al.*, “Aloin isoforms (A and B) selectively inhibits proteolytic and deubiquitinating activity of papain like protease (PLpro) of SARS-CoV-2 in vitro,” *Sci. Rep.*, vol. 12, no. 1, p. 2145, 2022, doi: 10.1038/s41598-022-06104-y.

[63] G. Liu *et al.*, “ISG15-dependent activation of the sensor MDA5 is antagonized by the SARS-CoV-2 papain-like protease to evade host innate immunity,” *Nat. Microbiol.*, vol. 6, no. 4, pp. 467–478, 2021, doi: 10.1038/s41564-021-00884-1.

[64] J. B. J. Ward *et al.*, “Ursodeoxycholic acid and lithocholic acid exert anti-inflammatory actions in the colon,” *Am. J. Physiol. Liver Physiol.*, vol. 312, no. 6, pp. G550–G558, Mar. 2017, doi: 10.1152/ajpgi.00256.2016.

[65] F. Kong, X. Niu, M. Liu, and Q. Wang, “Bile acids LCA and CDCA inhibited porcine deltacoronavirus replication in vitro,” *Vet. Microbiol.*, vol. 257, p. 109097, 2021, doi: https://doi.org/10.1016/j.vetmic.2021.109097.

[66] R. Strollo and P. Pozzilli, “DPP4 inhibition: Preventing SARS-CoV-2 infection and/or progression of COVID-19?,” *Diabetes. Metab. Res. Rev.*, vol. 36, no. 8, p. e3330, Nov. 2020, doi: https://doi.org/10.1002/dmrr.3330.

[67] S. B. Solerte, A. Di Sabatino, M. Galli, and P. Fiorina, “Dipeptidyl peptidase-4 (DPP4) inhibition in COVID-19,” *Acta Diabetol.*, vol. 57, no. 7, pp. 779–783, 2020, doi: 10.1007/s00592-020-01539-z.

[68] G. Iacobellis, “COVID-19 and diabetes: Can DPP4 inhibition play a role?,” *Diabetes Res. Clin. Pract.*, vol. 162, Apr. 2020, doi: 10.1016/j.diabres.2020.108125.

[69] S. M. Fred *et al.*, “Antidepressant and Antipsychotic Drugs Reduce Viral Infection by SARS-CoV-2 and Fluoxetine Shows Antiviral Activity Against the Novel Variants in vitro ,” *Frontiers in Pharmacology* , vol. 12. 2022, [Online]. Available: https://www.frontiersin.org/articles/10.3389/fphar.2021.755600.

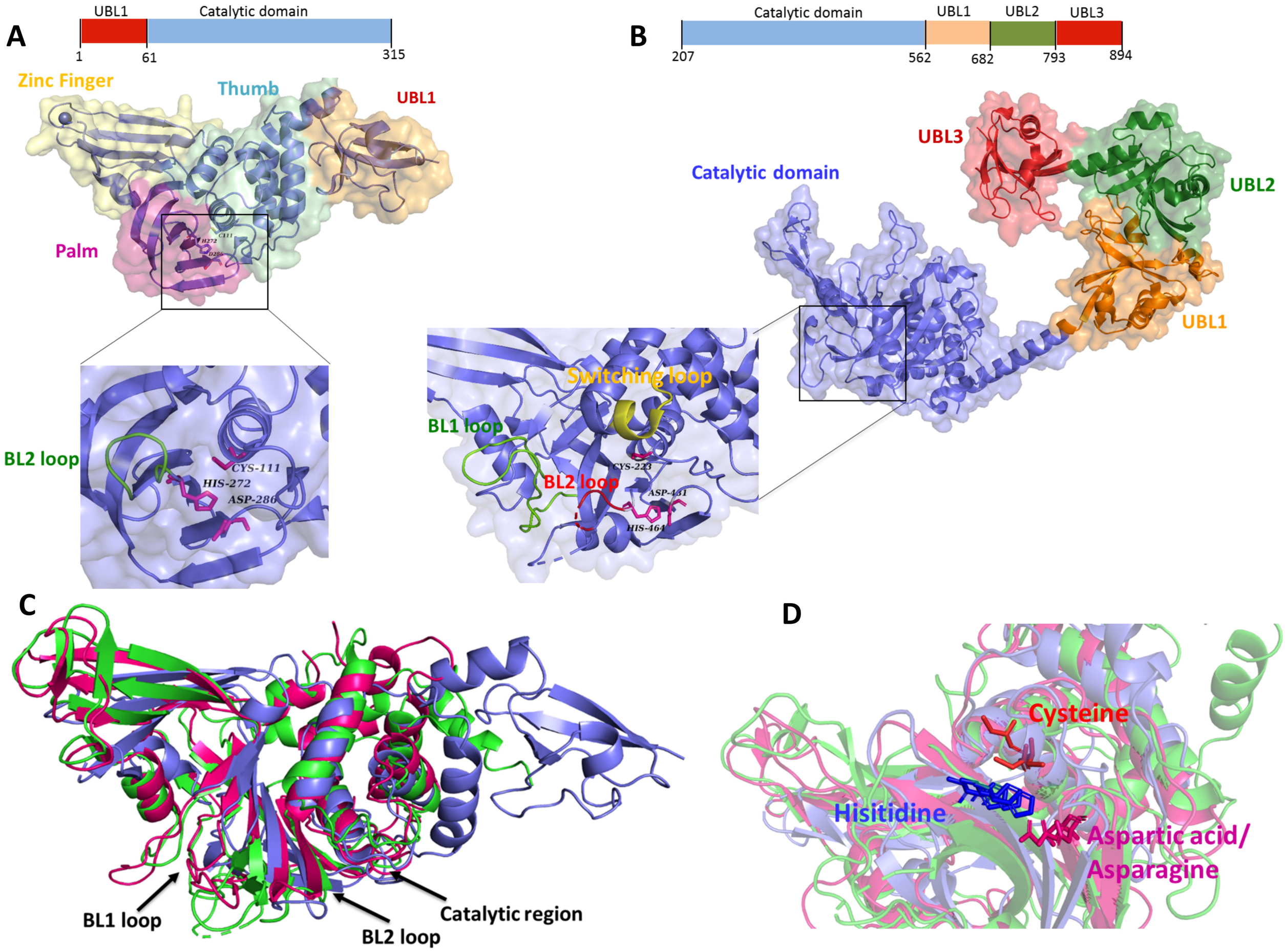
A
UBL1
Catalytic domain
1
61
315
Zinc Finger
Thumb
UBL1
Palm
C111
H272
D286
BL2 loop
CYS-111
HIS-272
ASP-286
B
Catalytic domain
UBL1
UBL2
UBL3
207
562
682
793
894
UBL3
Catalytic domain
UBL2
UBL1
Switching loop
BL1 loop
CYS-223
BL2 loop
ASP-431
HIS-464
C
BL1 loop
BL2 loop
Catalytic region
D
Cysteine
Hisitidine
Aspartic acid/
Asparagine

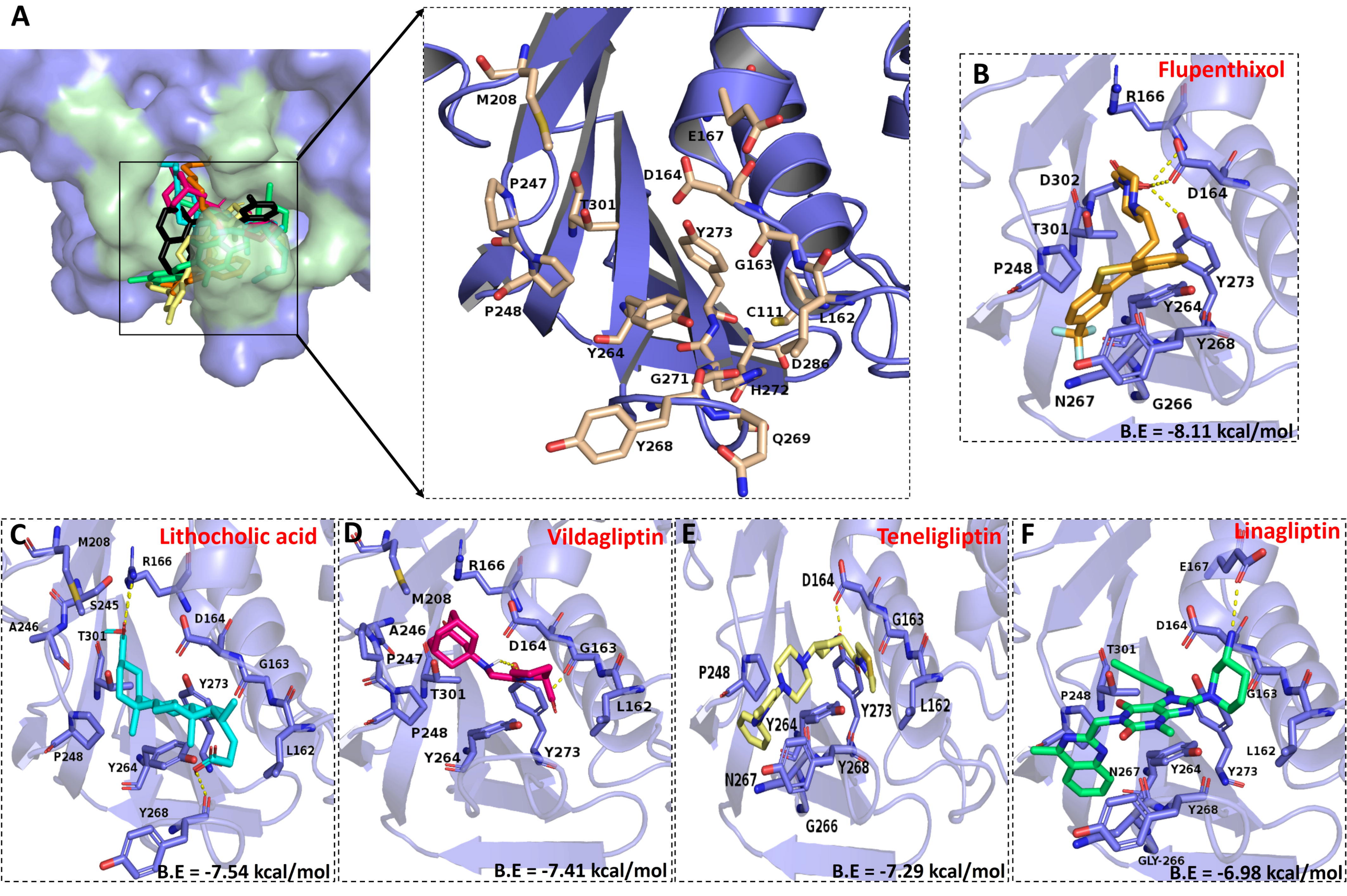
A
M208
E167
D164
P247
T301
Y273
G163
P248
C111
L162
Y264
D286
G271
H272
Y268
Q269
B
Flupenthixol
R166
D302
D164
T301
P248
Y273
Y264
Y268
N267
G266
B.E = -8.11 kcal/mol
C
Lithocholic acid
M208
R166
S245
A246
T301
D164
G163
Y273
P248
Y264
L162
Y268
B.E = -7.54 kcal/mol
D
Vildagliptin
R166
M208
A246
D164
G163
P247
T301
L162
P248
Y264
Y273
B.E = -7.41 kcal/mol
E
Teneligliptin
D164
G163
P248
Y264
Y273
L162
N267
Y268
G266
B.E = -7.29 kcal/mol
F
Linagliptin
E167
D164
T301
G163
P248
L162
N267
Y264
Y273
Y268
GLY-266
B.E = -6.98 kcal/mol

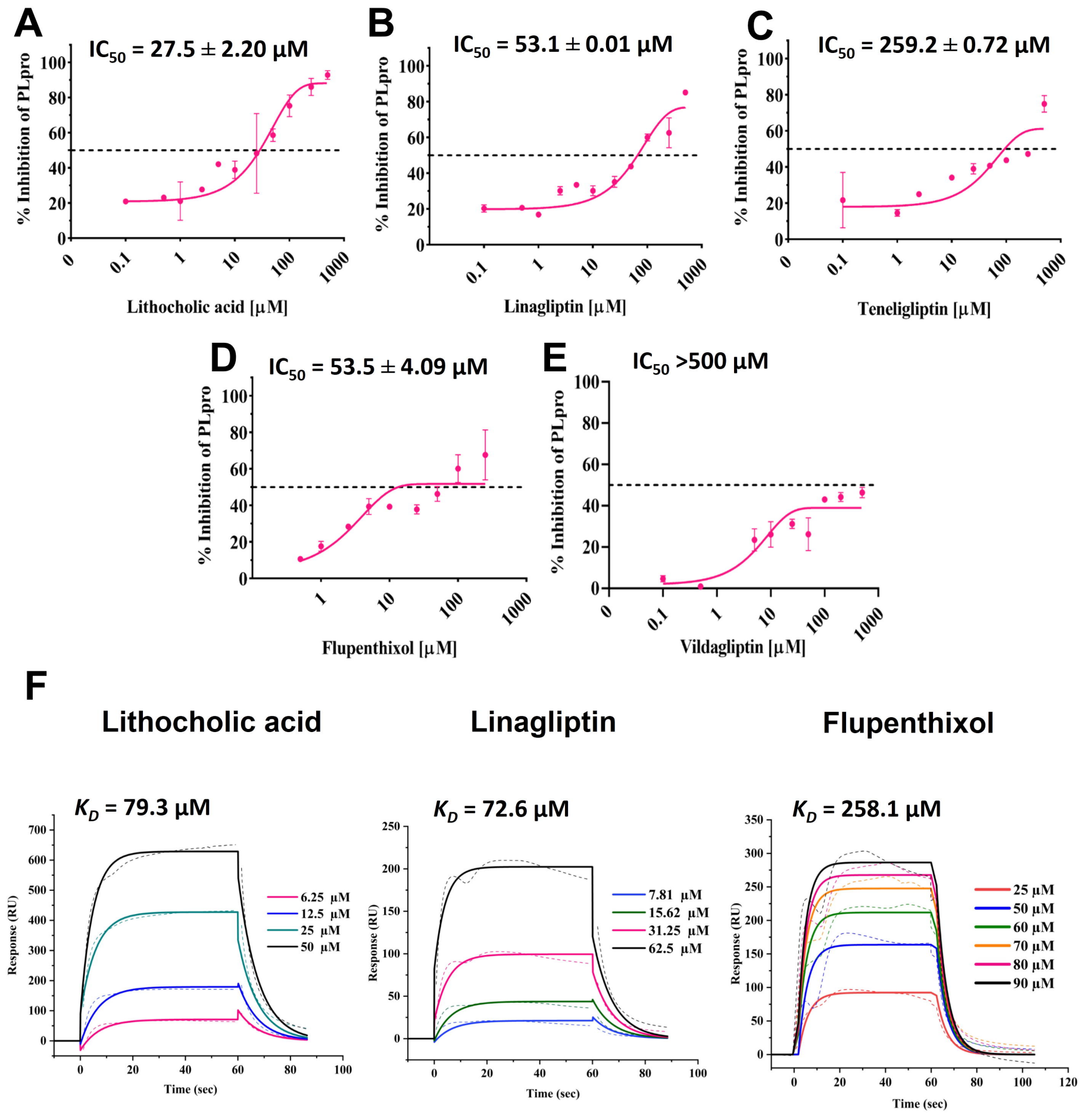
A
IC50 = 27.5 ± 2.20 μM
% Inhibition of PLpro
Lithocholic acid [μM]
B
IC50 = 53.1 ± 0.01 μM
% Inhibition of PLpro
Linagliptin [μM]
C
IC50 = 259.2 ± 0.72 μM
% Inhibition of PLpro
Teneligliptin [μM]
D
IC50 = 53.5 ± 4.09 μM
% Inhibition of PLpro
Flupenthixol [μM]
E
IC50 >500 μM
% Inhibition of PLpro
Vildagliptin [μM]
F
Lithocholic acid
KD = 79.3 μM
6.25 μM
12.5 μM
25 μM
50 μM
Response (RU)
Time (sec)
Linagliptin
KD = 72.6 μM
7.81 μM
15.62 μM
31.25 μM
62.5 μM
Response (RU)
Time (sec)
Flupenthixol
KD = 258.1 μM
25 μM
50 μM
60 μM
70 μM
80 μM
90 μM
Response (RU)
Time (sec)

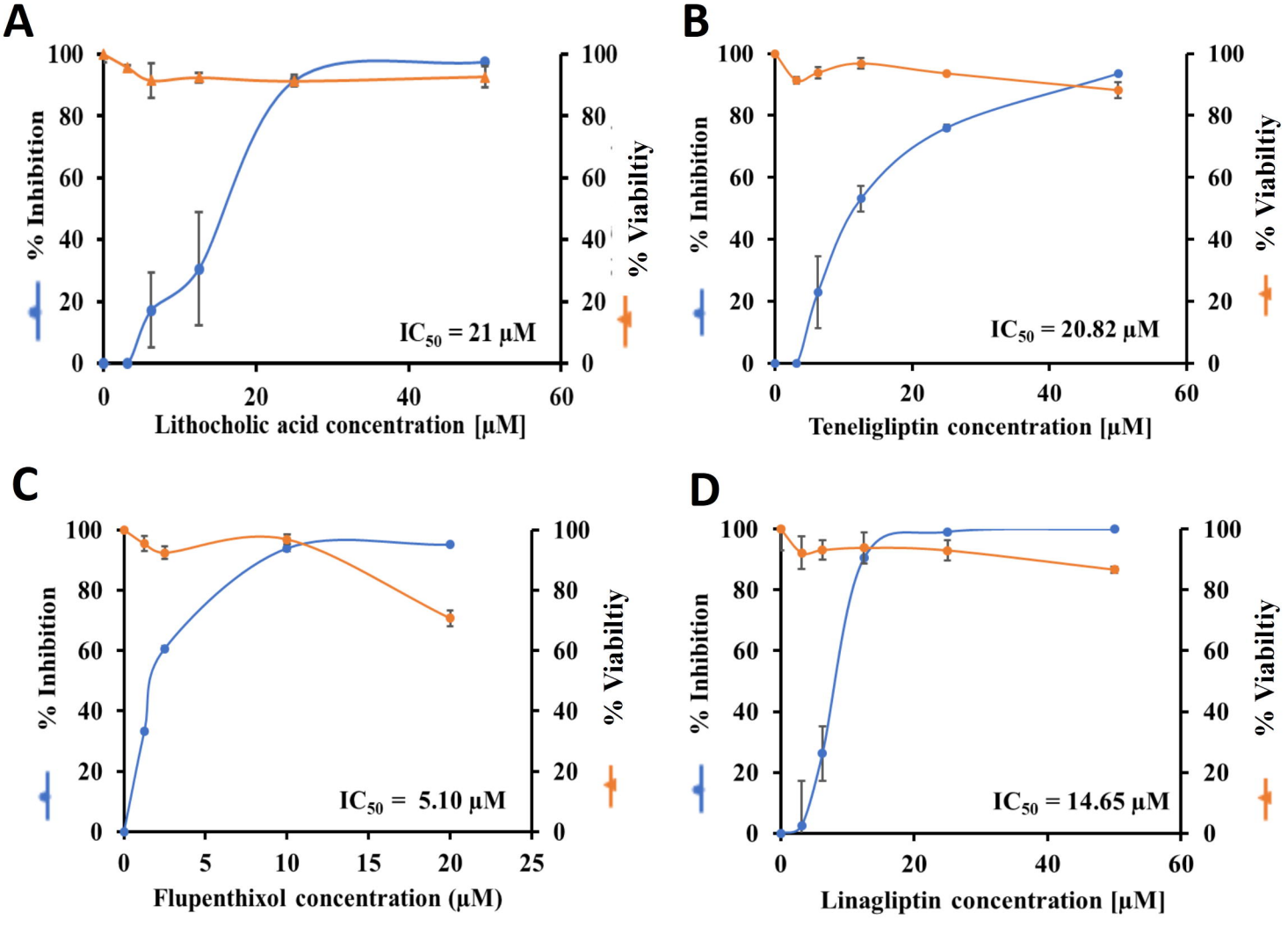
A
% Inhibition
% Viabiltiy
IC50 = 21 µM
Lithocholic acid concentration [µM]
B
% Inhibition
% Viabiltiy
IC50 = 20.82 µM
Teneligliptin concentration [µM]
C
% Inhibition
% Viabiltiy
IC50 = 5.10 µM
Flupenthixol concentration (µM)
D
% Inhibition
% Viabiltiy
IC50 = 14.65 µM
Linagliptin concentration [µM]

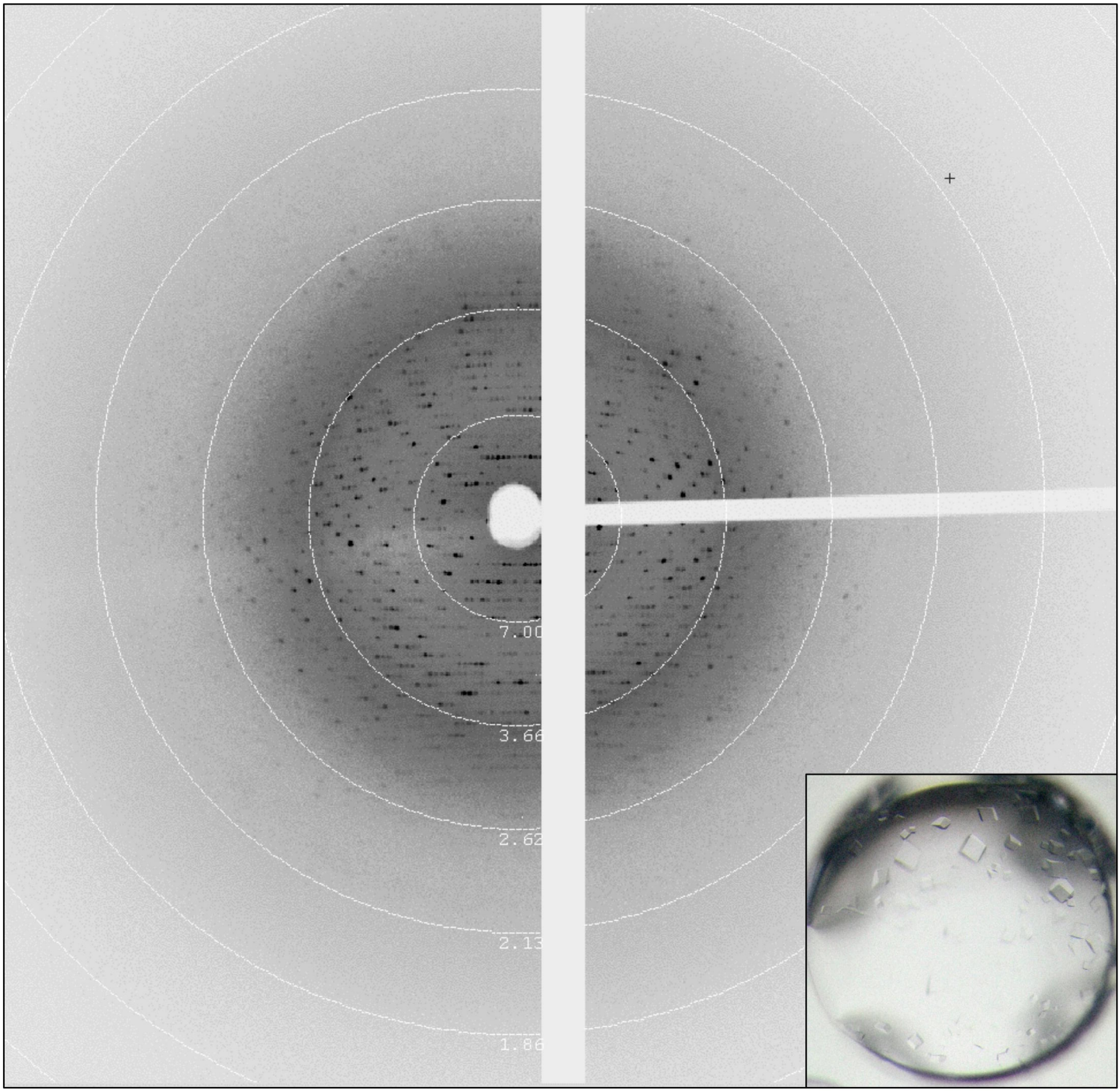
7.00
3.66
2.62
2.13
1.86